1-30-2013

Eigenfunction expansion of the time and space-dependent neutron survival probability equation

Ryan J. Kamm

Ryan J Kamm

Candidate

Nuclear Engineering

Department

This thesis is approved, and it is acceptable in quality and form for publication:

Approved by the Thesis Committee:

Dr. Anil K. Prinja , Chairperson

Dr. Robert D. Busch

Dr. Gary W. Cooper

Eigenfunction Expansion of the Time and Space-Dependent Neutron Survival Probability Equation

by

Ryan J Kamm

B.S., Nuclear Engineering, University of New Mexico, 2005

THESIS

Submitted in Partial Fulfillment of the
Requirements for the Degree of

Master of Science
Nuclear Engineering

The University of New Mexico

Albuquerque, New Mexico

December, 2012

Dedication

To the educators that are the University of New Mexico Department of Nuclear Engineering for making one of the most significant and appreciated impacts on the fundamental shape of my adult life.

Acknowledgments

While anything that I manage to accomplish is the result of the entirety of the momentum of the universe, and while I am consciously grateful for the way that seems to turn out, this is apparently not the place for such an acknowledgement. As such, there are a few individuals that the universe has produced in my vicinity for which I am particularly grateful insofar as the marked impact that they've visited on this avenue of my life, and therefore this body of work.

As the dedication reads, the faculty and staff of the Nuclear Engineering department that saw me through my undergraduate studies is owed a great deal more than they've been given. That said, even against the backdrop of such an outstanding cadre of people, I regard the impact of one especially dearly. Dr. Robert Busch showed me immeasurable kindness and consideration, facilitating the completion of my studies in a timely and uncompromised manner, and placing me well for a job immediately thereafter; not to mention, more than one meal and invaluable ping pong lessons. I owe you.

There is a sizable collection of truly outstanding people who I was lucky enough to work with at LANL, and I am forever grateful for the things I learned while working with them. In particular, Shean Monahan taught me a great deal about how humans behave and the importance of understanding the inevitability of that behavior, no matter how many procedures, rules, or mores are in place. More importantly, he showed me the strength of honesty and constitution in a time and environment where they were strangely unpopular. His generosity and commitment to excellence is second only to his talent with impressions. I owe you.

And finally, I'd like to acknowledge Dr. Anil Prinja for reigniting my enthusiasm in academia and seeing me through the travails of being a part-time graduate student. His appreciation for rigor and genuine passion for this work is obvious and inspiring. Were it not for his prodding, I'd still be torturing myself with Microsoft Office® products. I owe you.

Eigenfunction Expansion of the Time and Space-Dependent Neutron Survival Probability Equation

by

Ryan J Kamm

B.S., Nuclear Engineering, University of New Mexico, 2005

M.S., Nuclear Engineering, University of New Mexico, 2012

Abstract

Owing to their inherent complexity, stochastic neutron transport problems are often examined by either using highly simplified models to make solutions more accessible, or at the cost of significant computational effort for problems demanding higher accuracy than such simplified models afford.

In this work, solutions to stochastic transport equations of varying complexity are developed to examine a particular quantity of interest, the neutron survival probability. Using these solutions, the behavior of the survival probability is characterized throughout a wide range of parameters to better inform expectations as the complexity of the problem is increased.

First, the survival probability is modeled in an infinite medium. This provides insight into the relationship between the survival probability and the passage of survival time, the effective multiplication factor of the system, and the number of factorial moments of fission multiplicity preserved in the equation.

A steady-state diffusion equation is then solved semi-analytically in an one-dimensional slab, expanding understanding of the behavior of the survival probability and providing a benchmark for other space-dependent solutions. Additional steady-state solutions are produced by recognizing that the survival probability is well-approximated by the first eigenfunction of the linear portion of the equation. Not only is strong agreement observed with the semi-analytical solution, extension to other geometries is made accessible and the impact that varying geometry has on the survival probability is demonstrated.

Finally, solutions to the time and space-dependent survival probability diffusion equation are computed using an eigenfunction expansion technique. By comparison to the available semi-analytical steady-state solutions, as well as the known "initial" condition, the eigenfunction expansion technique demonstrates the capacity to produce solutions of arbitrary accuracy throughout the available parameter space. Extension to other geometries and multi-dimensional problems is performed, showing the broad capabilities of the technique as well as exploring facets of its performance. Additionally, a linear stability analysis of the equilibrium solution produced by the eigenfunction expansion technique is performed, rigorously demonstrating the stability of the associated solutions.

Contents

List of Figures

List of Tables

Chapter 1

Introduction

Inherent in the derivation of deterministic neutron transport equations is the assumption that the neutron population is large enough that fluctuations in that population about the mean may be ignored. This assumption holds well for many applications, including power reactor operation and assembly of critical experiments in the presence of a strong neutron source.

There are, however, important applications wherein no such sizable population can be credited with overshadowing deviations from the mean that result from the inherently probabilistic nature of nuclear reactions. Examples include the study of nuclear criticality accidents and assembly of critical experiments in the presence of a weak neutron source. In studying such phenomena, a knowledge of the probability of having a discrete, but arbitrary, number of neutrons in a given volume is essential [1]. For this reason stochastic neutron transport equations have been developed.

The difference between treating a neutron population stochastically, rather than deterministically, can drastically affect the pulse timing of burst reactors, the magnitude of an exposure associated with a criticality accident, and characteristics of other important phenomena. Hansen [2] noted that the neutron population in a

given supercritical configuration either can, or can not, be described by standard deterministic kinetics equation depending on whether or not the configuration was assembled in the presence of a "strong" or "weak" neutron source. By developing a point model of the probability that a neutron will sponsor a persistent chain reaction, he developed a somewhat qualitative definition of "strong" and "weak" neutron populations and showed that predictions of systems based on deterministic reactor kinetics equations can differ greatly from those resulting from stochastic treatment of the problem. Fortunately, the degree to which a population is governed by stochastic and deterministic behavior is thoroughly quantifiable. Prinja and Souto [3] rigorously demonstrated the transition of the neutron population from stochastic to deterministic behavior based on the source strength and multiplicative properties of the system.

Recognizing the need for a complete and modern treatment of stochastic neutron transport, Bell [4] developed an equation for the probability of finding an arbitrary number of neutrons in a given volume at a given time in the future as a result of one neutron existing with a given position and velocity at some initial time. Though Bell was the first to make use of the space- and energy-dependent forms of the equation, that Bell and Pál[5] independently derived probability distribution generating functions has caused the equation to be commonly referred to as the Pál-Bell equation.

Despite its mathematical complexity, the importance of the Pál-Bell equation is well appreciated. Of particular interest is a quantity that can be extracted from the Pál-Bell equation known as the survival probability. The survival probability is simply the complement of the extinction probability, which is the probability that zero neutrons will exist in a given volume, at some time in the future, as a result of one neutron existing with a given position and velocity at some initial time. As such, the survival probability does not provide information about the number of neutrons that will likely exist as a result of the initial neutron beyond that it is non-zero. Bell

and Lee [6] showed that the derivation of the survival probability equation is possible from first principles as well.

Though there may be a seeming sparseness of information associated with having lost information about the specific number of neutrons in the population, valuable physical insight can be gleaned from the survival probability equation. By noting that the only way that a neutron and its progeny can persist as time tends towards infinity is by being part of a divergent chain, it can be seen that the steady-state form of the survival probability equation provides what is coined the probability of initiation (POI). Clearly, the POI can only be non-zero for supercritical systems. In considering the time-dependent case, probability distributions in time of the initiation of the first divergent neutron chain in a system can be generated, which is instrumental in understanding the burst characteristics of the system being studied. Given its utility, the survival probability equation warrants investigation.

While simpler than the full Pál-Bell equation, the survival probability equation is extremely complex, resembling a standard adjoint transport equation with additional nonlinear terms. To wrest solutions from the equation, simplifications such as point models have been introduced, the contribution of nonlinear terms of degree higher than two has been ignored (referred to as the quadratic approximation), and some examinations have been restricted to the steady-state case. These simplifications are necessarily lacking in completeness, and hence a more expansive technique is desirable. While the complete time-dependent survival probability equation has been implemented in LANL's S_n code, PARTISN [7], it is computationally expensive and hence leaves room for the development of well sorted approximate solution to the problem with sufficient completeness.

The implementation in PARTISN was something of a conclusion to Bell's positing that an S_n code could be developed to solve the time-dependent survival probability equation. Bell and Lee documented the development of such a code [6] for the time-

independent case and confirmed, at least qualitatively, that the shape of the POI should be well characterized by the fundamental mode of an eigenfunction expansion of the linear portion of the equation for systems sufficiently close to criticality, as Bell had previously posited [4].

In this work, the efficacy of eigenfunction expansion (EFE) as a technique to arrive at solutions to the time-dependent survival probability equation will be examined. In doing so, the validity of Bell's posit will be quantified, and the scope increased to include significantly supercritical systems. To make the assessment more focused, the diffusion approximation in wide use in deterministic transport problems will be developed for the survival probability equation so that the exact eigenfunctions that result can be exploited for mathematical expediency. Ramsey and Hutchens [8] recently examined such a survival probability diffusion equation, though no eigenfunction expansion was performed. There,"a simple trial function/single-point collocation approach" was used, though nonlinear terms beyond the quadratic were neglected.

In addition to the development of the EFE technique, a number of lumped models, some analytical and some numerical, as well as a spatially-resolved semi-analytical equilibrium solution, will be developed and examined. Lumped models are so-called as they account for spatial effects in an averaged, simplified sense, and they are very useful in approximating the behavior of a system under certain simplifying assumptions. Additionally, they can be useful as benchmarks for related models in that the solutions to a more complex model can be reduced to those of the analytical lumped models, validating the associated numerical routines.

To assess the ability of EFE to accurately and efficiently model the survival probability, comparisons of its results will be drawn against those for the various analytical and semi-analytical benchmarks. With the EFE technique benchmarked, extension to various geometries, including cylinders, spheres, and two-dimensional slabs, will be demonstrated as well.

Chapter 2

Survival Probability Equations

2.1 The Pál-Bell Equation

Central to stochastic neutron transport theory is the probability of finding specific numbers of neutrons in a phase space of interest. As such, it is useful to define a quantity, $p_n\left(\mathrm{R}, t_f; \vec{r}, \hat{\Omega}, E, t\right)$, as the probability that a neutron with position $\vec{r}$, direction $\hat{\Omega}$, energy E, at time t will lead to n neutrons in an element of space, angle, and energy phase space R at time t_f. Equations for p_n may be formulated from first collision probabilities by writing them in terms of the probability that the initial particle has a collision in R before t_f, times the probability that that collision leads to n neutrons in R at t_f, plus the probability that the initial particle does not have a collision and leads to n neutrons in R at t_f. The latter probability can only be non-zero when n is either zero or one. Here, in following Bell's development [4], it will be assumed that the neutron population is monoenergetic, that neutrons emerge from collisions isotropically, and that there are no delayed neutron precursors. This being the case, the number distribution satisfies :

$$
\begin{aligned}
p_n\left(\mathrm{R}, t_f; \vec{r}, \hat{\Omega}, t\right) = & \left[\int_0^{l(s_b;s_t)} \Sigma_T\left(\vec{r}+s\hat{\Omega}, t+\tfrac{s}{v}\right) e^{-\int_0^s \Sigma_T\left(\vec{r}+s'\hat{\Omega}, t+\frac{s'}{v}\right) ds'} ds\right] \cdot \\
& \cdot \Bigg[\delta_{n0} c_0\left(\vec{r}+s\hat{\Omega}, t+\tfrac{s}{v}\right) + \\
& + c_1\left(\vec{r}+s\hat{\Omega}, t+\tfrac{s}{v}\right) \int_{4\pi} p_n\left(\mathrm{R}, t_f; \vec{r}+s\hat{\Omega}, \hat{\Omega}', t+\tfrac{s}{v}\right) \frac{d\hat{\Omega}'}{4\pi} + \\
& + c_2\left(\vec{r}+s\hat{\Omega}, t+\tfrac{s}{v}\right) \cdot \\
& \cdot \int_{4\pi} \int_{4\pi} \sum_{m=0}^{n} p_m\left(\mathrm{R}, t_f; \vec{r}+s\hat{\Omega}, \hat{\Omega}', t+\tfrac{s}{v}\right) \cdot \\
& \cdot p_{n-m}\left(\mathrm{R}, t_f; \vec{r}+s\hat{\Omega}, \hat{\Omega}'', t+\tfrac{s}{v}\right) \frac{d\hat{\Omega}'}{4\pi} \frac{d\hat{\Omega}''}{4\pi} + \\
& + c_3\left(\vec{r}+s\hat{\Omega}, t+\tfrac{s}{v}\right) \cdots \Bigg] + \\
& + \delta_{n0} \mathbb{H}\left[s_t - s_b\right] e^{-\int_0^{s_b} \Sigma_T\left(\vec{r}+s'\hat{\Omega}, t+\frac{s'}{v}\right) ds'} + \\
& + \delta_{n0} \mathbb{H}\left[s_b - s_t\right]_{\vec{r}+s_t\hat{\Omega}, \hat{\Omega} \notin \mathrm{R}} e^{-\int_0^{s_t} \Sigma_T\left(\vec{r}+s'\hat{\Omega}, t+\frac{s'}{v}\right) ds'} + \\
& + \delta_{n1} \mathbb{H}\left[s_b - s_t\right]_{\vec{r}+s_t\hat{\Omega}, \hat{\Omega} \in \mathrm{R}} e^{-\int_0^{s_t} \Sigma_T\left(\vec{r}+s'\hat{\Omega}, t+\frac{s'}{v}\right) ds'}
\end{aligned} \tag{2.1}
$$

where :

$$
s_t = v\left(t_f - t\right) \tag{2.2}
$$

$$
l\left(s_b; s_t\right) = \begin{cases} s_b & \text{if } s_b \leq s_t \\ s_t & \text{if } s_t < s_b \end{cases} \tag{2.3}
$$

Here, s_b is the distance the particle must travel to reach the system boundary, Σ_T is the total macroscopic cross-section, s is the measure of the length of l travelled, v is the neutron velocity (which Bell set to unity in his derivation), c_j is the probability

that j neutrons will emerge from a collision, δ_{ni} is the Kronecker delta function, and $\mathbb{H}$ is the Heaviside function. Being that negative particle quantities are nonphysical, p_n equals 0 for $n < 0$.

Introducing a generating function allows the series of n differential-difference equations to be combined into a single equation. This is accomplished by multiplying Eq. (2.1) by z^n and summing over n from zero to ∞. The generating function is defined by the following equation, where for convenience, the explicit dependence on R and t_f will be dropped :

$$G\left(z;\vec{r},\hat{\Omega},t\right) = \sum_{n=0}^{\infty} z^n p_n\left(\vec{r},\hat{\Omega},t\right) \tag{2.4}$$

As can be seen, this admits a significant simplification of the terms associated with collisions which result in an increase in the number of neutrons :

$$\begin{aligned} G\left(z;\vec{r},\hat{\Omega},t\right) = &\left[\int_0^{l(s_b;s_t)} \Sigma_T\left(\vec{r}+s\hat{\Omega},t+\tfrac{s}{v}\right) e^{-\int_0^s \Sigma_T\left(\vec{r}+s'\hat{\Omega},t+\frac{s'}{v}\right)ds'} ds\right]\cdot \\ &\cdot\Bigg[c_0\left(\vec{r}+s\hat{\Omega},t+\tfrac{s}{v}\right)+ \\ &+c_1\left(\vec{r}+s\hat{\Omega},t+\tfrac{s}{v}\right)\cdot\int_{4\pi} G\left(z;\vec{r}+s\hat{\Omega},\hat{\Omega}',t+\tfrac{s}{v}\right)\frac{d\hat{\Omega}'}{4\pi}+ \\ &+\sum_{j=2}^{J} c_j\left(\vec{r}+s\hat{\Omega},t+\tfrac{s}{v}\right)\cdot\left(\int_{4\pi} G\left(z;\vec{r}+s\hat{\Omega},\hat{\Omega}',t+\tfrac{s}{v}\right)\frac{d\hat{\Omega}'}{4\pi}\right)^j\Bigg]+ \\ &+\mathbb{H}\left[s_t-s_b\right] e^{-\int_0^{s_b}\Sigma_T\left(\vec{r}+s'\hat{\Omega},t+\frac{s'}{v}\right)ds'}+ \\ &+\mathbb{H}\left[s_b-s_t\right]_{\vec{r}+s_t\hat{\Omega},\hat{\Omega}\notin \mathrm{R}} e^{-\int_0^{s_t}\Sigma_T\left(\vec{r}+s'\hat{\Omega},t+\frac{s'}{v}\right)ds'}\Bigg]+ \\ &+\mathbb{H}\left[s_b-s_t\right]_{\vec{r}+s_t\hat{\Omega},\hat{\Omega}\in \mathrm{R}} z e^{-\int_0^{s_t}\Sigma_T\left(\vec{r}+s'\hat{\Omega},t+\frac{s'}{v}\right)ds'} \end{aligned} \tag{2.5}$$

Here, J is the maximum number of particles that can emerge from a collision. Evaluating Eq. (2.5) for $G\left(z;\vec{r}+\Delta s\hat{\Omega},\hat{\Omega},t+\frac{\Delta s}{v}\right)$ replaces the lower integration

limits in the collision probability term with Δs, and hence the value corresponds to the lesser of the track lengths from Δs to the system boundary, or from Δs along $s\hat{\Omega}$ until time reaches t_f. Subtracting Eq. (2.5), which corresponds to the value along the entire $s\hat{\Omega}$ track length, leaves a value corresponding to the track length up to Δs. Driving Δs to zero allows for the formation of a non-linear partial differential equation that defines the behavior of the generating function at the point $\vec{r}$:

$$\hat{\Omega}\cdot\nabla G+\frac{1}{v}\frac{\partial G}{\partial t}=\Sigma_T\left(\vec{r},t\right)\left[G\left(z;\vec{r},\hat{\Omega},t\right)-\sum_{j=0}^{J}c_j\left(\vec{r},t\right)G_0\left(z;\vec{r},t\right)^j\right] \tag{2.6}$$

with the final condition :

$$\begin{aligned} G\left(z;\vec{r},\hat{\Omega},t_f\right) &= z & \vec{r},\hat{\Omega}\in \mathrm{R} \\ &= 1 & \vec{r},\hat{\Omega}\notin \mathrm{R} \end{aligned} \tag{2.7}$$

and the boundary condition :

$$G\left(z;\vec{r}_b,\hat{\Omega},t\right) = 1 \qquad \hat{\Omega}\cdot\vec{n}>0 \tag{2.8}$$

where G_0 is here defined :

$$G_0\left(z;\vec{r},t\right)=\int_{4\pi}G\left(z;\vec{r},\hat{\Omega}',t\right)\frac{d\hat{\Omega}'}{4\pi} \tag{2.9}$$

A more convenient equation, in that it may be expressed in terms of the measurable nuclear properties of cross-sections and the factorial moments of fission multiplicities, is possible for the complement of the generating function :

$$-\hat{\Omega}\cdot\nabla g-\frac{1}{v}\frac{\partial g}{\partial t}=\Sigma_T\left(\vec{r},t\right)\left[1-g\left(z;\vec{r},\hat{\Omega},t\right)-\sum_{j=0}^{J}c_j\left(\vec{r},t\right)\left(1-g_0\left(z;\vec{r},t\right)\right)^j\right] \tag{2.10}$$

where :

$$g\left(z;\vec{r},\hat{\Omega},t\right) = 1 - G\left(z;\vec{r},\hat{\Omega},t\right) \tag{2.11}$$

$$g_0\left(z;\vec{r},t\right) = \int_{4\pi} g\left(z;\vec{r},\hat{\Omega}',t\right)\frac{d\hat{\Omega}'}{4\pi} \tag{2.12}$$

$$c_0 = \frac{\Sigma_C}{\Sigma_T} + p_0\frac{\Sigma_F}{\Sigma_T} \tag{2.13}$$

$$c_1 = \frac{\Sigma_S}{\Sigma_T} + p_1\frac{\Sigma_F}{\Sigma_T} \tag{2.14}$$

$$c_2 = p_2\frac{\Sigma_F}{\Sigma_T} \tag{2.15}$$

$$\vdots$$

$$c_j = p_j\frac{\Sigma_F}{\Sigma_T} \tag{2.16}$$

Here, Σ_C is the macroscopic capture cross-section, Σ_S is the macroscopic scattering cross-section, Σ_F is the macroscopic fission cross-section, and p_j is the probability that a fission will release j neutrons. Because of the relationships between the various c_j and the macroscopic cross-sections, the first couple of terms in the summation in Eq. (2.10) may be expanded and rearranged to produce an equation in terms of those cross-sections :

$$-\hat{\Omega}\cdot\nabla g - \frac{1}{v}\frac{\partial g}{\partial t} = -\Sigma_T g + \Sigma_S g_0 + \Sigma_F\left[1 - \sum_{j=0}^{J} p_j\left(1-g_0\right)^j\right] \tag{2.17}$$

To recast Eq. (2.17) as a function of the factorial moments of the fission multiplicities, expansion of the summation term by way of the binomial theorem must first be performed :

$$-\hat{\Omega}\cdot\nabla g-\frac{1}{v}\frac{\partial g}{\partial t}=-\Sigma_T g+\Sigma_S g_0+\Sigma_F\left[1-\sum_{j=0}^{J}p_j\sum_{k=0}^{j}\frac{(-1)^{j-k}j!}{(j-k)!k!}{g_0}^{j-k}\right] \tag{2.18}$$

Expanding and regrouping the terms in the double summation allows for the more desirable grouping by order of the associated nonlinearity of the terms. The resulting coefficients are the factorial moments being sought :

$$-\hat{\Omega}\cdot\nabla g-\frac{1}{v}\frac{\partial g}{\partial t}=-\Sigma_T g+\Sigma_S g_0+\Sigma_F\left[\bar{\nu}g_0-\sum_{j=2}^{J}\frac{(-1)^j\chi_j}{j!}{g_0}^j\right] \tag{2.19}$$

where:

$$\bar{\nu}=\sum_{j=0}^{J}jp_j \tag{2.20}$$

$$\chi_j=\sum_{k=j}^{J}\frac{k!}{(k-j)!}p_k \tag{2.21}$$

Here, $\bar{\nu}$ is the average number of neutrons emitted per fission and $\chi_j/j!$ is the average number of j-tuplet neutron groups emitted per fission.

2.2 The Survival Probability Equation

The present aim is to determine the probability that a neutron with position $\vec{r}$, direction $\hat{\Omega}$, at time t, will lead to a non-zero number of neutrons in R at time t_f (i.e., the survival probability). In calculating this quantity, it is useful to observe that the survival probability is simply the complement of the extinction probability. The extinction probability is the probability that a neutron with position $\vec{r}$, direction $\hat{\Omega}$, at time t will lead to zero neutrons in R at time t_f. To arrive at the extinction probability, z is set to zero in Eq. (2.4) :

$$G\left(z;\vec{r},\hat{\Omega},t\right)=p_0+zp_1+z^2p_2+\cdots+z^np_n$$

$$G\left(0;\vec{r},\hat{\Omega},t\right)=p_0 \tag{2.22}$$

The survival probability is therefore simply g with z equal to zero. For convenience, P will be taken to represent the survival probability going forward :

$$P\left(\vec{r},\hat{\Omega},t\right)\equiv g\left(0;\vec{r},\hat{\Omega},t\right) \tag{2.23}$$

The survival probability therefore satisfies the following equation :

$$-\hat{\Omega}\cdot\nabla P-\frac{1}{v}\frac{\partial P}{\partial t}=-\Sigma_T P+\Sigma_S P_o+\Sigma_F\left[\bar{\nu}P_o-\sum_{j=2}^{J}\frac{(-1)^j\chi_j}{j!}{P_o}^j\right] \tag{2.24}$$

with the final condition :

$$\begin{aligned} P\left(\vec{r},\hat{\Omega},t_f\right) &= 1 && \vec{r},\hat{\Omega}\in \mathrm{R} \\ &= 0 && \vec{r},\hat{\Omega}\notin \mathrm{R} \end{aligned} \tag{2.25}$$

and the boundary condition :

$$P\left(\vec{r}_b,\hat{\Omega},t\right) = 0 \qquad \hat{\Omega}\cdot\vec{n}>0 \tag{2.26}$$

where :

$$P_o\left(z;\vec{r},t\right)=\int_{4\pi}P\left(z;\vec{r},\hat{\Omega}',t\right)\frac{d\hat{\Omega}'}{4\pi} \tag{2.27}$$

Eq. (2.24) resembles an adjoint Boltzmann transport equation with additional nonlinear terms that account for the neutron multiplicities that result from fission. The resemblance to a deterministic transport equation comes as no surprise given that the same physical processes dictate the behavior of the subject particle, and spurs the expectation that solutions to the survival probability equation ought to resemble those for the neutron importance functions of the system.

2.3 Existing Formulations of the Survival Probability Equation

It is worthwhile to explore the relationship that Eq. (2.24) has with similar equations developed in the foundational works of stochastic neutron transport.

For a neutron chain to survive as t_f grows toward infinity, the system must be supercritical and the neutrons that exist in R as a result of the initial particle must be part of a divergent chain. Setting the derivative with respect to time equal to zero in Eq. (2.24) therefore produces an equation for the POI, P_∞ :

$$\hat{\Omega}\cdot\nabla P_\infty = \Sigma_T P_\infty\left(\vec{r},\hat{\Omega}\right) - \Sigma_S P_\infty\left(\vec{r}\right) + \Sigma_F\left[\bar{\nu}P_\infty\left(\vec{r}\right) - \sum_{j=2}^{J}\frac{(-1)^j\chi_j}{j!}P_\infty\left(\vec{r}\right)^j\right] \tag{2.28}$$

Eq. (2.28) is very similar to the equation that Bell and Lee derived from first principles in documenting the development of their S_n code designed to solve the time-independent survival probability equation. Relaxing the assumption that particles emerge from scattering collisions isotropically recovers their equation :

$$\hat{\Omega}\cdot\nabla P_\infty = \Sigma_T P_\infty\left(\vec{r},\hat{\Omega}\right) - \int_{4\pi}\Sigma_S\left(\vec{r},\hat{\Omega}'\rightarrow\hat{\Omega}\right)P_\infty\left(\vec{r},\hat{\Omega}'\right)d\hat{\Omega}' + \\ +\Sigma_F\left[\bar{\nu}P_\infty\left(\vec{r}\right) - \sum_{j=2}^{J}\frac{(-1)^j\chi_j}{j!}P_\infty\left(\vec{r}\right)^j\right] \tag{2.29}$$

A 0-D lumped model description of the survival probability, Q, wherein a uniform spatial profile is assumed, can be readily extracted from Eq. (2.24) by removing the dependence on $\vec{r}$ and $\hat{\Omega}$:

$$\frac{1}{v}\frac{dQ}{dt} = \Sigma_T Q - \Sigma_S Q - \Sigma_F \left[\bar{\nu} Q - \sum_{j=2}^{J} \frac{(-1)^j \chi_j}{j!} Q^j\right] \tag{2.30}$$

Neglecting the fission terms in Eq. (2.30) resulting from J greater than two recovers the analogous point-kinetics equation for the survival probability derived by Hansen in his examination of neutron chains in the presence of weak neutron sources.

Both a diffusion theory analog to the steady-state survival probability equation, Eq. (2.29), and the 0-D lumped model, Eq. (2.30), will be examined as complexity of the problem is increased toward the full time and space-dependent problem.

Chapter 3

The Diffusion Approximation

It is the objective of this work to examine the ability of the eigenfunction expansion technique to describe the space and time-dependent behavior of the survival probability. Because this is to be something of a feasibility study of that approach, it is desirable that the eigenfunctions be readily obtained, preferably without requiring additional numerical effort. To this end, the diffusion approximation that is often applied to deterministic transport problems will be applied to Eq. (2.24) so that the exact eigenfunctions of the resulting equation for special geometries may be exploited, divesting the survival probability of its dependence on angle and increasing the accessibility of solutions.

3.1 The Diffusion Approximation of the Survival Probability Equation

A standard approach will be used for reducing the transport equation, Eq. (2.24), to a diffusion equation [9] [10] [11].

First, it will be assumed that the medium is uniform in composition and unchanging in time so that the cross-sections are not functions of space within the medium, or of time. Therefore, the way in which the survival probability behaves in the constant medium does not change with time, but only with the difference between the "current" time, t, and the final time, t_f, which will be referred to hereafter as the survival time, τ. Moreover, the survival time will be normalized to units of neutron lifetimes, t_l, and the assumption that scattering is isotropic will be relaxed :

$$\hat{\Omega}\cdot\nabla P-\Sigma_A\frac{\partial P}{\partial\tau}=\Sigma_T P-\int_{4\pi}\Sigma_S\left(\hat{\Omega}'\cdot\hat{\Omega}\right)P\left(\hat{\Omega}'\right)d\hat{\Omega}'- \\ -\Sigma_F\left[\bar{\nu}P_o-\sum_{j=2}^{J}\frac{(-1)^j\chi_j}{j!}{P_o}^j\right] \tag{3.1}$$

where :

$$\tau=\frac{(t_f-t)}{t_l} \tag{3.2}$$

$$t_l=\frac{1}{v\Sigma_A} \tag{3.3}$$

Eq. (3.1) is a function of an angle dependent survival probability, P, and an angle independent survival probability, P_o. In an effort to remove the dependence on angle so as to have the complexity reduced, each term in Eq. (3.1) is integrated over all solid angles. In doing so, it becomes useful to define a vector survival probability current, $\vec{P}$:

$$\vec{P}\left(\vec{r},t\right)=\int_{4\pi}\hat{\Omega}P\left(\vec{r},\hat{\Omega},t\right)\frac{d\hat{\Omega}}{4\pi} \tag{3.4}$$

Physically, the survival probability current is the net contribution to the survival probability that results from particle streaming in $\hat{\Omega}$ at $\vec{r}$. By extension, $\vec{P}\cdot\hat{n}$ is

the rate at which the survival probability changes through a unit area normal to $\hat{n}$. Mathematically, it is simply the integral of the product of the angle dependent survival probability and the associated angle over all solid angles.

For ease of manipulation, the fission terms will be lumped together as an isotropically emitting source, F_o before Eq. (3.1) is integrated over all angles :

$$\int_{4\pi}\left[\hat{\Omega}\cdot\nabla P-\Sigma_A\frac{\partial P}{\partial\tau}\right]d\hat{\Omega}=\int_{4\pi}\left[\Sigma_T P-\int_{4\pi}\Sigma_S\big(\hat{\Omega}'\cdot\hat{\Omega}\big)P\big(\hat{\Omega}'\big)d\hat{\Omega}'-F_o\right]d\hat{\Omega} \tag{3.5}$$

where :

$$F_o=\Sigma_F\left[\bar{\nu}P_o-\sum_{j=2}^{J}\frac{(-1)^j\chi_j}{j!}{P_o}^j\right] \tag{3.6}$$

By taking advantage of the definitions of $\vec{P}$ and P_o and the fact that $\hat{\Omega}\cdot\nabla P=\nabla\cdot\hat{\Omega}P$, Eq. (3.5) may be significantly simplified :

$$\nabla\cdot\vec{P}-\Sigma_A\frac{\partial P_o}{\partial\tau}=\Sigma_A P_o-F_o \tag{3.7}$$

Unfortunately, Eq. (3.7) is also a function of two distinct quantities; the survival probability current, $\vec{P}$, and the angle-independent survival probability, P_o. Multiplying Eq. (3.1) by $\frac{\hat{\Omega}}{4\pi}$ before integrating, in an effort to develop an equation for the survival probability current, results in another distinct quantity, $\int_{4\pi}\hat{\Omega}\hat{\Omega}Pd\hat{\Omega}$:

$$\frac{1}{4\pi}\nabla\cdot\int_{4\pi}\hat{\Omega}\hat{\Omega}Pd\hat{\Omega}-\Sigma_A\frac{\partial\vec{P}}{\partial\tau}=\Sigma_T\vec{P}-\bar{\mu}\Sigma_S\vec{P} \tag{3.8}$$

Here, $\bar{\mu}$ is the average scattering angle cosine. Because the integral of $\hat{\Omega}$ over all angles is zero, the angle independent source term in Eq. (3.8) vanished.

Clearly, proceeding to multiply the equation by $\hat{\Omega}$ and integrating over all solid angles in hopes of solving for the newly created quantities will just generate new

quantities and the process will not conclude. To bring closure to the problem at hand, it will be assumed that the survival probability is only weakly dependent on angle. Specifically, it will be assumed that the survival probability is sufficiently well-characterized as linearly anisotropic :

$$P\left(\vec{r},\hat{\Omega},\tau\right) \cong P_{_0}\left(\vec{r},\tau\right) + 3\hat{\Omega}\cdot\vec{P}\left(\vec{r},\tau\right) \tag{3.9}$$

Investigation of Eq. (3.9) by way of multiplying by $\frac{1}{4\pi}$ and $\frac{\hat{\Omega}}{4\pi}$, respectively, and then integrating over all angles demonstrates mathematical consistency. Multiplying Eq. (3.9) by $\frac{1}{4\pi}$ and integrating over all angles recovers the definition of $P_{_0}$:

$$\int_{4\pi} P\frac{d\hat{\Omega}}{4\pi} = P_{_0}\cancelto{1}{\int_{4\pi}\frac{d\hat{\Omega}}{4\pi}} + 3\vec{P}\cancelto{0}{\int_{4\pi}\hat{\Omega}\frac{d\hat{\Omega}}{4\pi}} = P_{_0} \tag{3.10}$$

Multiplying Eq. (3.9) by $\frac{\hat{\Omega}}{4\pi}$ and then integrating over all angles recovers the definition of survival probability current, $\vec{P}$:

$$\int_{4\pi}\hat{\Omega}P\frac{d\hat{\Omega}}{4\pi} = P_{_0}\cancelto{0}{\int_{4\pi}\hat{\Omega}\frac{d\hat{\Omega}}{4\pi}} + 3\vec{P}\cancelto{1/3}{\int_{4\pi}\hat{\Omega}\hat{\Omega}\frac{d\hat{\Omega}}{4\pi}} = \vec{P} \tag{3.11}$$

Substituting the linearly anisotropic survival probability from Eq. (3.9) into the survival probability current equation, Eq. (3.8) and integrating gives :

$$\frac{1}{4\pi}\nabla\left[P_{_0}\cancelto{4\pi/3}{\int_{4\pi}\hat{\Omega}\hat{\Omega}\frac{d\hat{\Omega}}{4\pi}} + 3\vec{P}\cancelto{0}{\int_{4\pi}\hat{\Omega}\hat{\Omega}\hat{\Omega}d\hat{\Omega}}\right] - \Sigma_{_A}\frac{\partial\vec{P}}{\partial\tau} = \left(\Sigma_{_T} - \bar{\mu}\Sigma_{_S}\right)\vec{P} \tag{3.12}$$

To arrive at an expression for $\vec{P}$ in terms of P_0 from Eq. (3.12), it will be assumed that the rate at which the survival probability current varies with survival time can be neglected :

$$\frac{1}{3}\nabla P_0 - \Sigma_A \frac{\partial \cancelto{0}{\vec{P}}}{\partial \tau} = (\Sigma_T - \bar{\mu}\Sigma_S)\,\vec{P}$$

which yields Fick's Law :

$$\vec{P} = D\nabla P_0 \tag{3.13}$$

where :

$$D = \frac{1}{3\Sigma_{tr}} \tag{3.14}$$

$$\Sigma_{tr} = \Sigma_T - \bar{\mu}\Sigma_S \tag{3.15}$$

Here, D is the diffusion coefficient and Σ_{tr} is the macroscopic transport cross-section.

Finally, a single equation for the angle independent survival probability can be realized by substituting Eq. (3.13) into Eq. (3.7) :

$$D\nabla^2 P_0 - \Sigma_A \frac{\partial P_0}{\partial \tau} = \Sigma_A P_0 - \Sigma_F \left[\bar{\nu} P_0 - \sum_{j=2}^{J} \frac{(-1)^j \chi_j}{j!} {P_0}^j\right] \tag{3.16}$$

3.2 The Survival Probability Diffusion Equation

It is the survival probability diffusion equation that will be the central focus of this work. Having no further need for the distinction between angle-dependent and -independent survival probabilities, the subscript notation will be dropped, and P will be used to refer to the angle-independent survival probability described by Eq. (3.16) for ease of notation. Some rearranging and combining of terms produces a more amenable form :

$$-\frac{\partial P}{\partial \tau} + L^2 \nabla^2 P = (1 - k_\infty)\, P + \frac{\Sigma_F}{\Sigma_A} \sum_{j=2}^{J} \frac{(-1)^j \chi_j}{j!} P^j \tag{3.17}$$

with the "initial" condition :

$$\begin{aligned} P(\vec{r}, 0) &= 1 && \vec{r} \in \mathrm{R} \\ &= 0 && \vec{r} \notin \mathrm{R} \end{aligned} \tag{3.18}$$

and the boundary condition :

$$P(\vec{r}, \tau) = 0 \qquad \vec{r} \notin \mathrm{R} \tag{3.19}$$

where :

$$L^2 = \frac{D}{\Sigma_A} \tag{3.20}$$

$$k_\infty = \frac{\bar{\nu} \Sigma_F}{\Sigma_A} \tag{3.21}$$

Here, L is the diffusion length and k_∞ is the infinite multiplication factor.

The "initial" condition states that the probability that a particle will lead to at least one particle in R if no time is allowed to pass is unity for particles in R. This is a self-consistent statement in that if the particle is not allowed time to move and interact with the medium, it will necessarily remain.

The boundary condition simply states that there is no probability that a particle introduced beyond the boundary of the system will lead to one or more in the system. While a more accurate treatment of diffusion approximation problems is possible by way of the familiar Marshak boundary conditions, the purpose of the current work is primarily to examine the efficacy of an eigenfunction expansion technique. The boundary condition is therefore chosen to be Dirichlet to make examination of the performance of the technique more straightforward.

With the survival probability diffusion equation now well posed for general geometries and material compositions, it is worth observing that the solution will only converge with passing survival time if at least the quadratic factorial moment is included. This is intuitive in that if only the linear terms are preserved, Eq. (3.17) is analogous to an equation for the flux in a deterministic transport problem, except the leakage term acts as a net gain. If such a system were supercritical, as the systems that are the concern of this work are, the flux would diverge in time. Hence, so would the survival probability. Moreover, as will be shown later, linearized versions of Eq. (3.17) can be used to assess the stability of nonzero steady-state solutions.

Chapter 4

A Time-Dependent 0-D Lumped Model

To develop a general sense of how the survival probability behaves, a significantly simplified form of the equation, one for which the probability is uniform throughout the medium, will first be examined. The only way that the survival probability could be the same everywhere in a medium is if that medium were infinite in extent. As such, an equation for the survival probability in a hypothetical infinite medium will be developed.

The obvious shortcoming of this approach is that it cannot inform as to any spatial behavior. Still, a qualitative understanding of system characteristics, such as how quickly the survival probability converges to the POI, and rough estimates for the value of the survival probability as a function of various parameters (e.g., system excess reactivity, number of factorial moments included, and survival time), can be gleaned. In this way, an understanding of the relative impact that varying these parameters has on the system behavior can be begin to be developed to help inform expectations for other, less simplified models.

4.1 Development of a Spatially Uniform Lumped Model

Considering the survival probability in this hypothetical infinite medium, Q, eliminates the term with the Laplacian operator in Eq. (3.17) along with any dependence on $\vec{r}$. The result is the following nonlinear ordinary differential equation :

$$\frac{dQ}{d\tau} = (k_\infty - 1)\, Q(\tau) - \frac{k_\infty}{\bar{\nu}} \sum_{j=2}^{J} \frac{(-1)^j \chi_j}{j!} Q(\tau)^j \tag{4.1}$$

with the "initial" condition :

$$Q(0) = 1 \tag{4.2}$$

Obviously, the absence of the leakage term eliminates the loss associated with that phenomenon. To compensate for this, an artificial loss mechanism is introduced by substituting k_{eff} for k_∞ in an effort to account for finite-system effects :

$$\frac{dQ}{d\tau} = (k_{eff} - 1)\, Q(\tau) - \frac{k_{eff}}{\bar{\nu}} \sum_{j=2}^{J} \frac{(-1)^j \chi_j}{j!} Q(\tau)^j \tag{4.3}$$

4.1.1 Applying the Quadratic Approximation : Development of an Analytical Expression for a Time Dependent 0-D Lumped Model

Applying the quadratic approximation eliminates nonlinear terms of degree three and greater from Eq. (4.3). Because the quadratic form is a Bernoulli Equation, an analytical solution is possible. This solution can serve to benchmark the numerical solution scheme needed to solve Eq. (4.3) for greater degrees of nonlinearity.

First, the quadratic form (*i.e.*, $J = 2$) of Eq. (4.3) is recast by performing a change of variables :

$$W(\tau) = \frac{1}{Q(\tau)} \tag{4.4}$$

which yields :

$$\frac{dW}{d\tau} + \alpha W = \beta \tag{4.5}$$

with the "initial" condition :

$$W(0) = \frac{1}{Q(0)} = 1 \tag{4.6}$$

where :

$$\alpha = (k_{eff} - 1) \tag{4.7}$$

$$\beta = \frac{k_{eff}}{\bar{\nu}} \frac{\chi_2}{2!} \tag{4.8}$$

Using integrating factors and applying the "initial" condition readily yields an analytical solution for the quadratic approximation of Eq. (4.3) :

$$Q(\tau) = \frac{1}{\frac{1}{\rho}\frac{\chi_2/2!}{\bar{\nu}}(1 - e^{-\alpha\tau}) + e^{-\alpha\tau}} \tag{4.9}$$

where :

$$\rho = \frac{k_{eff} - 1}{k_{eff}} \tag{4.10}$$

Here, ρ is the system excess reactivity. Being that the ability of a multiplying system to propagate a neutron chain is tied to the effective multiplication factor of that system, so to is the survival probability of a neutron in that system. Physical intuition therefore suggests that the survival probability, and by extension the POI, ought to go as the excess reactivity of the system in which it is injected. Eq. (4.9) supports this intuition, and permits a well-quantified expectation of the magnitude of the POI without having to perform any numerical work :

$$\lim_{\tau\to\infty} Q(\tau) \equiv Q_\infty = \frac{1}{\frac{1}{\rho}\frac{\chi_2/2!}{\bar{\nu}}(1-\cancelto{0}{e^{-\alpha\tau}}) + \cancelto{0}{e^{-\alpha\tau}}}$$

$$Q_\infty = \rho\frac{\bar{\nu}}{\chi_2/2!} \tag{4.11}$$

Eq. (4.11) shows that the quadratic form of the survival probability equation has an equilibrium value directly proportional to the system excess reactivity. Because successively higher order nonlinear terms contribute less by virtue of being the product of both increasingly small physical constants and numbers less than one raised to increasing powers, Eq. (4.11) leads one to expect that the POI ought to roughly approximate the system excess reactivity, particularly for smaller excess reactivities where the higher order nonlinear terms contribute negligibly.

4.2 Numerical Results of the 0-D Lumped Model

All computations shown in this body of work are performed using scripts written for use with Matlab R2012a. The platform used is 64-bit and all values are double-precision floating-point numbers. All relative and absolute error tolerances for numerical integrations are the highest precision allowed by the platform used; the relative error tolerances are set to $2.2204 \cdot 10^{-14}$ and the absolute error tolerances are set to $4.4408 \cdot 10^{-16}$.

The medium is modeled as pure ^{235}U throughout all computations. All nuclear cross-sections, as well as the average number of neutrons emitted per fission, $\bar{\nu}$, are from Los Alamos National Laboratories' Nuclear Information Services. Specifically, the NJOY nuclear data processing system [12] processed ENDF/B-VII data [13] to generate the relevant nuclear data. This data was collapsed to a single energy group using the ^{235}U prompt neutron energy spectrum for weighting to coincide with the one-speed approximation applied in the development of the survival probability diffusion equation. The factorial moments of the fission multiplicities were computed using Eq. (2.21) and probabilities of n neutrons being emitted per fission corresponding to the aforementioned value of $\bar{\nu}$ [14]. The data used in the computations is summarized below in Table 4.1.

Table 4.1: Physical Constants

$N_{^{235}U}$ (^{235}U/barn $\cdot$ cm)	v (cm/sec)	σ_s (barn)	σ_c (barn)	σ_f (barn)
$4.8552 \cdot 10^{-2}$	$2.0137 \cdot 10^{9}$	6.1043	$5.0638 \cdot 10^{-2}$	1.2231
$\bar{\nu}$	$\chi_2/2!$	$\chi_3/3!$	$\chi_4/4!$	$\chi_5/5!$
2.750	3.076	1.772	0.564	0.007

Because the survival probability diffusion equation is numerically stiff, associated differential equations are solved throughout this work using a variable order solver based on the numerical differentiation formulas [15]. The solutions are considered to have converged on a steady-state solution when the maximum difference between the values for the survival probability at a given position differ by less than $4.4408 \cdot 10^{-16}$ between successive survival time steps.

The behavior of the survival probability for small survival times can be seen in Figure 4.1 for varying values of k_{eff} and J, as computed using the 0-D lumped model.

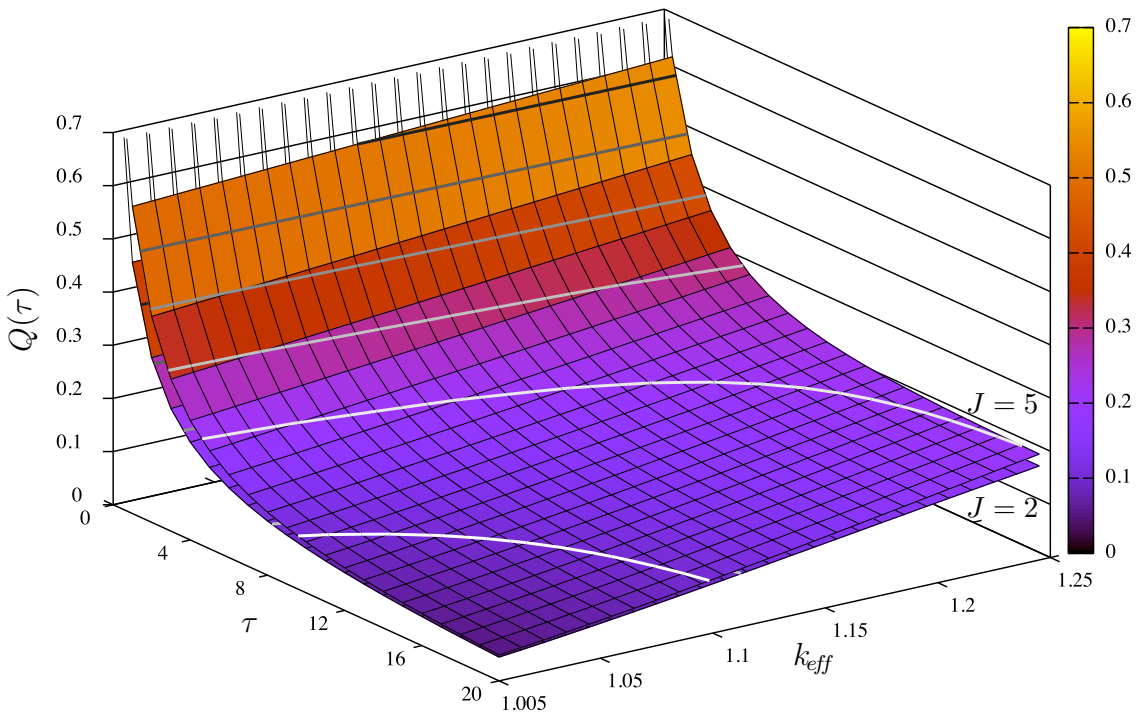

Figure 4.1: $Q(\tau)$ for Small Survival Times ($\tau \leq 20$)

Figure 4.1 shows that the survival probability decreases more rapidly, and to smaller values, for smaller values of k_{eff}, regardless of J. This makes intuitive sense as the likelihood that a particle will survive for a given duration is directly tied to the multiplicative properties of the system in which it is propagating.

It is also clear that there exists a substantial difference between the survival probability computed using the quadratic approximation ($i.e., J = 2$) and higher order nonlinearity for small survival times, and that the two become less disparate as the survival time tends toward infinity, particularly for smaller values of k_{eff}. This is as expected, given that the survival probability itself is diminishing with increasing survival time, and the importance of additional nonlinear terms in providing an accurate solution is greater for greater values of the survival probability.

It is worth noting that the numerical solutions for the 0-D survival probability with $J = 2$ are identical to those for the analytical solution to within the specified tolerances throughout the entire k_{eff} and τ phase space, granting a high degree of confidence in the numerical ODE solver used herein.

Even given the small survival times captured in Figure 4.1, the asymptotic approach of the survival probability toward the 0-D POI, Q_∞, can be seen for the higher values of k_{eff}. While the solution technique used to solve Eq. (4.3) converges on the POI with increasing survival time, the exact POI for the 0-D lumped model described by Eq. (4.3) is simply the real root of a J-degree polynomial between zero and one :

$$0 = \rho Q_\infty - \frac{1}{\bar{\nu}} \sum_{j=2}^{J} \frac{(-1)^j \chi_j}{j!} {Q_\infty}^j \tag{4.12}$$

As the examination of the analytical expression derived by applying the quadratic approximation showed, the POI is linearly proportional to the system excess reactivity.

Although the POI can be solved for directly for quadratic and cubic forms of the survival probability equation in an infinite medium, how much survival time must pass for the system to satisfy the steady-state convergence criteria and arrive at the POI can only be determined numerically. Both the POI and the corresponding "infinite" survival time, τ_∞, are shown in Figure 4.2. Whether the POI is computed using Eq. (4.3) with the established POI convergence criteria, or by finding the appropriate root of Eq. (4.12), the values for the POI computed are identical to within machine precision, inspiring further confidence in the accuracy of the numerical scheme used to solve Eq. (4.3).

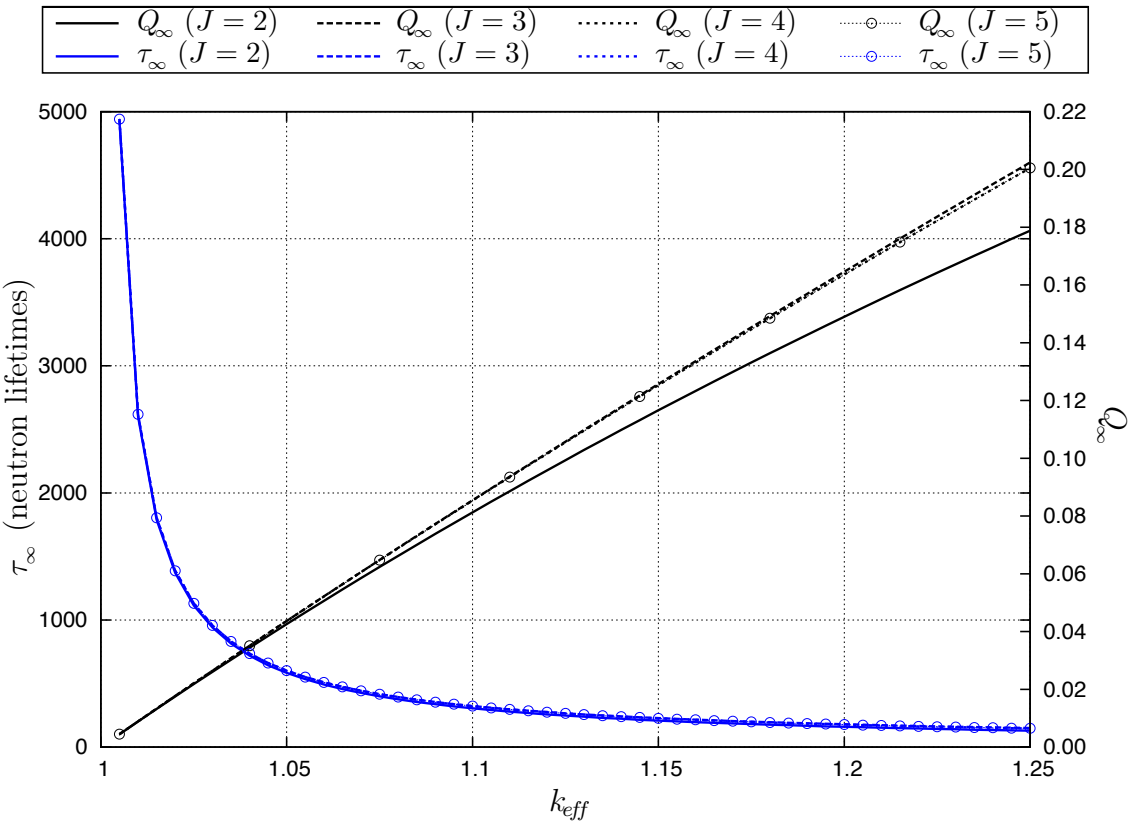

Figure 4.2: Q_∞ and τ_∞ for Varying k_{eff}

Figure 4.2 makes clear the need for higher order nonlinearity for accurately modeling higher values of the POI. It also shows that the survival time required for convergence is largely unaffected by the degree of nonlinearity of the survival probability equation, and almost purely a function of k_{eff}.

As an important aside, the nature of the variable order method implemented to solve Eq. (4.3) can somewhat obfuscate the convergence time by solving over larger intervals of survival time as the solution becomes asymptotic. To consistently resolve the survival time required to reach steady state to within a given value, in this case a single neutron lifetime, the degree of variability that the solver is allowed to use in adjusting the time step size may be fixed such that a step size cannot be greater than that value. This, however, comes at the cost of significant added computational run time. Because the resulting values for the survival probability are indistinguishable

given the scrutiny allowed by machine precision, the significantly increased speed of the unrestricted variable order solver is the tool of choice for all studies of this equation except for survival time to steady state.

While Figures 4.1 and 4.2 have provided a qualitative demonstration of the discrepancy introduced in computing the survival probability with truncated nonlinearity, a quantitative analysis provides the needed elucidation. To see the relative impact that varying the degree of nonlinearity of the equation has on the survival probability, the difference in a solution for a given degree of nonlinearity relative to the solution computed for full nonlinearity (i.e., $J = 5$), and therefore the most accurate, is plotted in Figure 4.3.

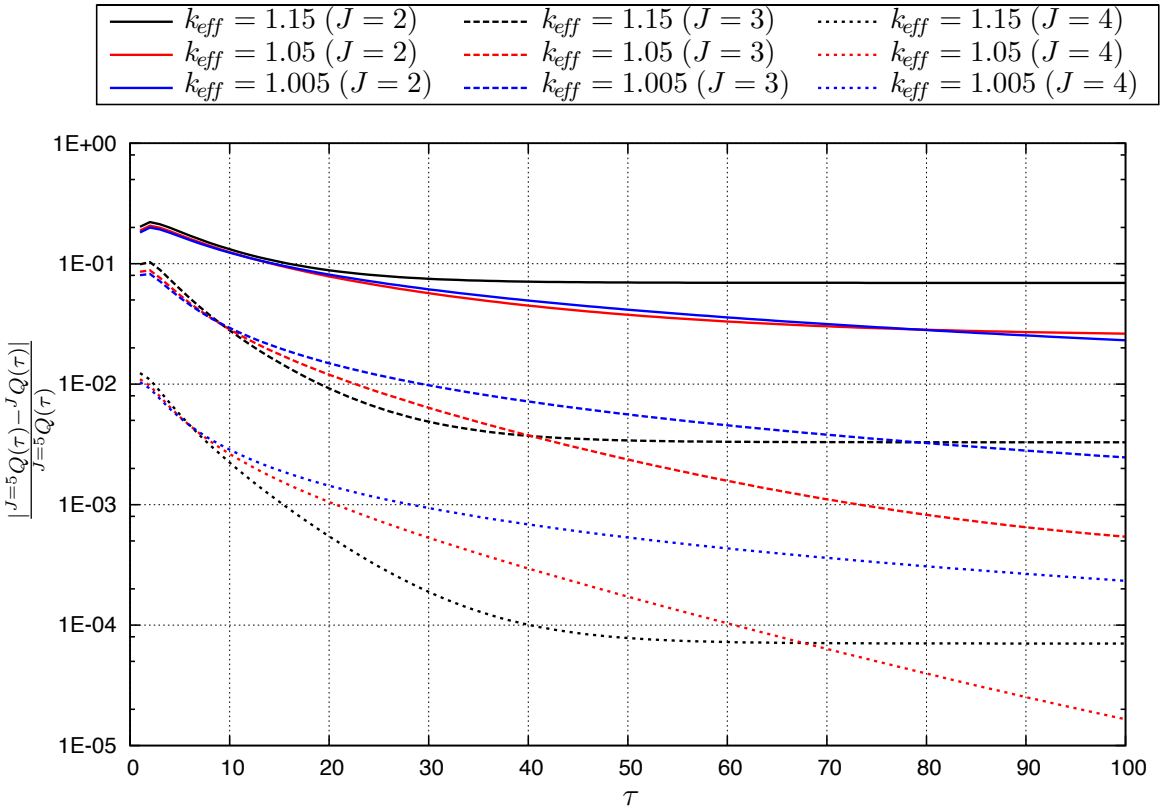

Figure 4.3: Error in $Q(\tau)$ Relative to the Fully Nonlinear $(J = 5)$ Solution

Because the "initial" condition requires that the survival probability be unity for zero survival time, it is to be expected that the impact of truncating the nonlinearity of the survival probability equation will be significant in early survival times, regardless of k_{eff}. Clearly, the higher order nonlinear terms are not significantly diminished in early survival times, as they aren't yet factors of numbers significantly less than one raised to increasing powers. In later time, the value of the survival probability continues to drop for lower values of k_{eff}, and therefore so does the relative error associated with truncation of the nonlinearity. This coincides with previous observations and reinforces that the importance of preserving higher degrees of nonlinearity is a function of the magnitude of the survival probability .

Figure 4.4 quantifies this impact for the steady-state case throughout a wide range of k_{eff}.

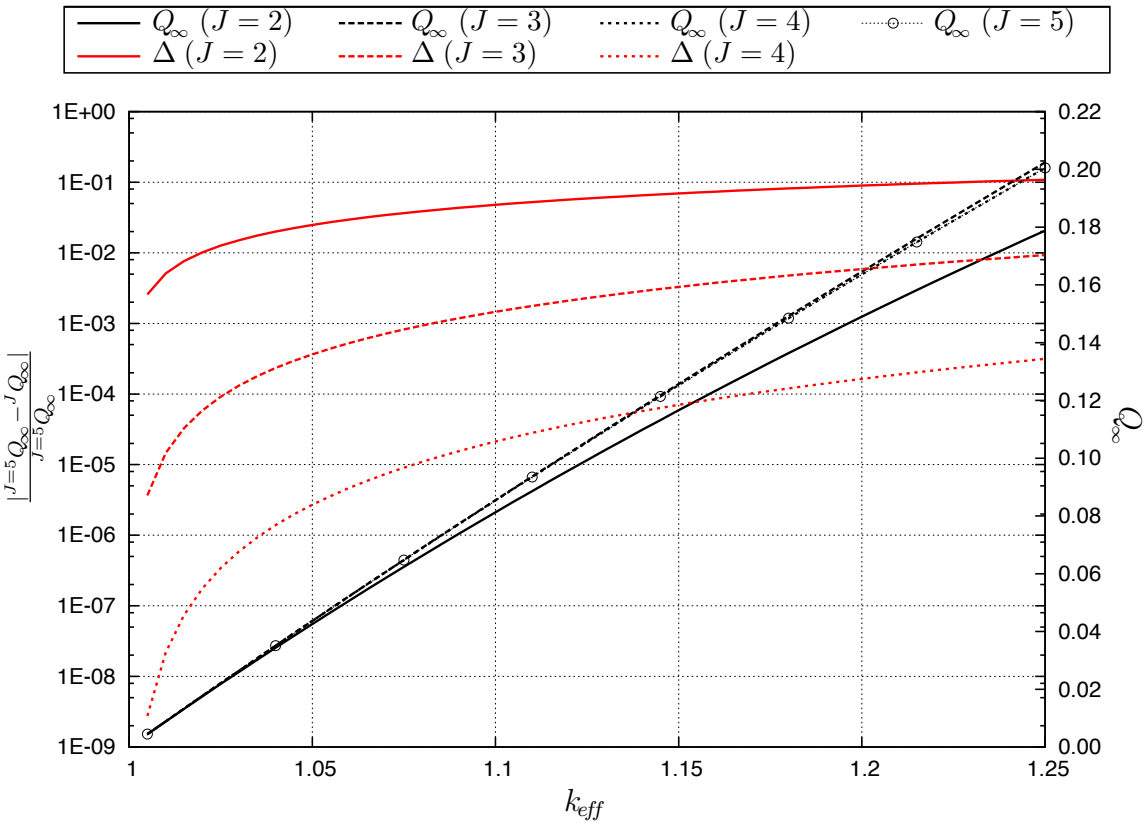

Figure 4.4: Q_∞ and Error in Q_∞ Relative to the Fully Nonlinear $(J = 5)$ Solution

4.3 Conclusions from the 0-D Lumped Model

Examination of the spatially uniform lumped model demonstrated a number of important characteristics of the survival probability. While the results presented in this chapter are those of a somewhat crudely lumped model, the trends and dependencies on various parameters informs expectations for solutions of less simplified models of the survival probability.

Using this simplification, both the temporal profile and magnitude of the survival probability were shown to exhibit significant dependence on the degree of nonlinearity of the survival probability equation, J. Examination of the survival probability equation reveals the rate of change of the survival probability and the magnitude of the POI vary linearly with k_{eff} and the system excess reactivity, respectively. The role that varying system k_{eff} plays in the associated solution accuracy is therefore that it informs the magnitude of the survival probability at a given point in time. Computing the survival probability with any variation in J then produces error in the value commensurate with the degree of nonlinearity truncation.

In short, setting $J = 2$ produces solutions which underestimate the survival probability by more than 10% for values of the survival probability greater than ~ 0.2. Setting $J = 3$ was found to produce solutions with errors of less than 1% for similar values. Clearly, higher order nonlinear terms are needed to accurately define the system behavior for higher values of the survival probability, such as for very small survival times and high excess reactivities.

Chapter 5

Space-Dependent Steady-State Solutions

While the 0-D lumped model was computationally inexpensive, and therefore preferable for helping to develop a general sense of the magnitude and temporal behavior of the survival probability, it is necessarily limited in its ability to inform. Though the "initial" condition requires that the survival probability be uniform throughout the medium, this is not the case in a finite medium for nonzero survival times.

To develop a sense of how the survival probability varies spatially, an examination of the profile of the space-dependent steady-state survival probability, $P_{\infty}(\vec{r})$, will be conducted. In so doing, an understanding of the shape of the POI as a function of k_{eff}, as well as the degree of nonlinearity of the equation, will be cultivated.

Though a direct analytical solution is not possible, a full spatial solution for the time-independent case in a one-dimensional slab can be found in implicit form, which can be readily evaluated using quadrature. Thusly, the shape of the POI is accessible. Bell and Lee qualitatively verified that the first eigenfunction (i.e., the fundamental mode) corresponding to the linear eigenvalue equation for an importance function of

a given system (i.e., the linear portion of the survival probability equation) is a "good approximation" of the POI for "slightly supercritical systems." [6] Expectations are therefore established for the examination to be undertaken here.

Because the POI may be solved for semi-analytically, the solutions can serve as a benchmark, facilitating a quantification of how well a fundamental mode approximation represents the POI for varying values of k_{eff} and degrees of nonlinearity, and against which a time and space-dependent eigenfunction expansion solution may be compared, at least at its steady state.

5.1 Development of a Semi-Analytical Solution

In considering the time-independent survival probability in a one-dimensional slab of thickness X, defining some coefficients for ease of notation allows Eq. (3.17) to be recast in the more compact form :

$$\frac{d^2 P_\infty}{dx^2} = \sum_{j=1}^{J} (-1)^j C_j {P_\infty}^j \tag{5.1}$$

with the boundary condition :

$$P_\infty \left(\pm \frac{X}{2} \right) = 0 \tag{5.2}$$

where :

$$C_1 = B_m^2 = \frac{k_\infty - 1}{L^2} \tag{5.3}$$

$$C_j = \frac{\Sigma_F}{D} \frac{\chi_j}{j!} \tag{5.4}$$

Here, B_m^2 is the material buckling of the medium.

A reduction in order of Eq. (5.1) allows for separation, which in turn allows for integration. First, a change of variables is performed :

$$q = \frac{dP_\infty}{dx} \tag{5.5}$$

By substituting q into Eq. (5.1) and dividing by q, an expression coupling two first order differential equations results :

$$\frac{1}{q}\frac{dq}{dx} = \frac{1}{q}\left(\sum_{j=1}^{J}(-1)^j C_j {P_\infty}^j\right)$$

$$\frac{dq}{dP_\infty} = \frac{1}{q}\left(\sum_{j=1}^{J}(-1)^j C_j {P_\infty}^j\right) \tag{5.6}$$

Eq. (5.6) can be separated and integrated :

$$\int q dq = \int \left(\sum_{j=1}^{J}(-1)^j C_j {P_\infty}^j\right) dP_\infty$$

$$\frac{q^2}{2} = \sum_{j=1}^{J}\frac{(-1)^j C_j}{j+1}{P_\infty}^{j+1} + \kappa_1 \tag{5.7}$$

Because $P_\infty(x)$ is symmetrical about the origin so that ${P_\infty}'(0) = q(0) = 0$, applying homogeneous boundary conditions allows for the constant of integration, κ_1, to be computed :

$$\frac{q(0)^{\cancel{2}^{0}}}{\cancel{2}} = \sum_{j=1}^{J}\frac{(-1)^j C_j}{j+1}P_\infty(0)^{j+1} + \kappa_1$$

$$\kappa_1 = -\sum_{j=1}^{J}\frac{(-1)^j C_j}{j+1}P_\infty(0)^{j+1} \tag{5.8}$$

By substituting Eq. (5.8) into Eq. (5.7), an expression for q in terms of P_∞ and $P_\infty(0)$ is recovered :

$$q = \pm\sqrt{2\sum_{j=1}^{J}\frac{(-1)^j C_j}{j+1}\left({P_\infty}^{j+1} - P_\infty(0)^{j+1}\right)} \tag{5.9}$$

The symmetry of the solution about the origin again informs the path to solution by providing that values of $P_\infty(x)$ from Eq. (5.9) for $x \geq 0$ alone create a complete solution. As such, only the negative values of q need be computed. Substituting the definition of q into Eq. (5.9) yields a separable nonlinear first order ordinary differential equation :

$$\frac{dP_\infty}{dx} = -\sqrt{2\sum_{j=1}^{J}\frac{(-1)^j C_j}{j+1}\left({P_\infty}^{j+1} - P_\infty(0)^{j+1}\right)}$$

$$dx = \frac{dP_\infty}{-\sqrt{2\sum_{j=1}^{J}\frac{(-1)^j C_j}{j+1}\left({P_\infty}^{j+1} - P_\infty(0)^{j+1}\right)}} \tag{5.10}$$

Integrating Eq. (5.10) produces an expression wherein the function being sought, $P_\infty(x)$, is a limit of integration. Hence, the solution is implicit :

$$\int_x^{X/2} dx = -\int_{P_\infty(x)}^{0} \frac{dP_\infty}{\sqrt{2\sum_{j=1}^{J}\frac{(-1)^j C_j}{j+1}\left({P_\infty}^{j+1} - P_\infty(0)^{j+1}\right)}}$$

$$\int_0^{P_\infty(x)} \frac{dP_\infty{}'}{\sqrt{2\sum_{j=1}^{J}\frac{(-1)^j C_j}{j+1}\left({P_\infty}'^{j+1} - P_\infty(0)^{j+1}\right)}} = \frac{X}{2} - x \tag{5.11}$$

Eq. (5.11) provides a means to compute the value of $P_\infty(x)$ for a given value of x, but only if one already knows the value at $x = 0$, $P_\infty(0)$. To find this value, it is useful to define, and then compute, a normalized survival probability :

$$y(x) = \frac{P_\infty(x)}{P_\infty(0)} \tag{5.12}$$

By substituting Eq. (5.12) into Eq. (5.11), an expression that lends itself to evaluation for the central value of the survival probability results :

$$\int_0^{y(x)} \frac{P_\infty(0)dy'}{\sqrt{2P_\infty(0)^2 \sum_{j=1}^{J} \frac{(-1)^j C_j}{j+1} \frac{P_\infty(0)^{j+1}}{P_\infty(0)^2} \left(y'^{j+1} - 1\right)}} - \frac{X}{2} + x = 0$$

$$\int_0^{y(x)} \frac{dy'}{\sqrt{2\sum_{j=1}^{J} \frac{(-1)^j C_j}{j+1} P_\infty(0)^{j-1} \left(y'^{j+1} - 1\right)}} - \frac{X}{2} + x = 0 \tag{5.13}$$

Setting $x = 0$ in Eq. (5.13) produces an implicit equation for $P_\infty(0)$:

$$\int_0^{1} \frac{dy'}{\sqrt{2\sum_{j=1}^{J} \frac{(-1)^j C_j}{j+1} P_\infty(0)^{j-1} \left(y'^{j+1} - 1\right)}} - \frac{X}{2} = 0 \tag{5.14}$$

By implementing a Newton-Raphson iteration scheme, $P_\infty(0)$ can be computed :

$$P_\infty^{k+1}(0) = P_\infty^{k}(0) - \frac{g\left(P_\infty^k(0)\right)}{g'\left(P_\infty^k(0)\right)} \quad \text{for } k = 0, 1, 2, \cdots \tag{5.15}$$

where :

$$g\left(P_\infty^k(0)\right) = \int_0^1 \left[2\sum_{j=1}^{J} \frac{(-1)^j C_j}{j+1} P_\infty^k(0)^{j-1} \left(y'^{j+1} - 1\right)\right]^{-1/2} dy' - \frac{X}{2} \tag{5.16}$$

$$g'\left(P_\infty^k(0)\right) = \int_0^1 \frac{\left[2\sum_{j=1}^{J} \frac{(-1)^j C_j}{j+1}\left(j-1\right) P_\infty^k(0)^{j-2}\left(y'^{j+1}-1\right)\right]}{-\frac{1}{2}\left[2\sum_{j=1}^{J} \frac{(-1)^j C_j}{j+1} P_\infty^k(0)^{j-1}\left(y'^{j+1}-1\right)\right]^{3/2}} dy' \tag{5.17}$$

By providing an initial guess for $P_\infty^1(0)$ and iterating on k, Eq. (5.15) will converge on a value for $P_\infty(0)$. Based on the discussion of the expected values for the survival probability that produced Eq. (4.11), the initial guess is set to the system excess reactivity.

With the value of $P_\infty(0)$ in hand, another Newton-Raphson iteration scheme can be implemented to solve Eq. (5.11) for $P_\infty\left(x\right)$ for varying values of x :

$$P_\infty^{k+1} = P_\infty^k - \frac{g\left(P_\infty^k\right)}{g'\left(P_\infty^k\right)} \quad \text{for } k = 0, 1, 2, \cdots \tag{5.18}$$

where :

$$g\left(P_\infty^k\right) = \int_0^{P_\infty^k} \left[2\sum_{j=1}^{J} \frac{(-1)^j C_j}{j+1}\left(P_\infty{}'^{j+1} - P_\infty(0)^{j+1}\right)\right]^{-1/2} dP_\infty{}' - \frac{X}{2} + x \tag{5.19}$$

$$g'\left(P_\infty^k\right) = \left[2\sum_{j=1}^{J} \frac{(-1)^j C_j}{j+1}\left(P_\infty^{k\,j+1} - P_\infty(0)^{j+1}\right)\right]^{-1/2} \tag{5.20}$$

5.2 A Fundamental Mode Approximation

To quantify how well the POI is represented by a fundamental mode approximation, ${}_{N=1}P_\infty$, an expression for that approximation must be developed. In contrast to the semi-analytical solution, this approach may be applied to general geometries, and will therefore be developed in such a way.

First, it is assumed that the POI is well represented by the first eigenfunction of an expansion of the linear portion of the survival probability equation :

$$_{N=1}P_{\infty}(\vec{r}) = A_1 R_1(\vec{r}) \tag{5.21}$$

where R_1 is a solution to :

$$\nabla^2 R_1 = -B_g^2 R_1 \tag{5.22}$$

(e.g., $A_1 \cos(B_g x)$, $A_1 J_0(B_g r)$, and $A_1 \frac{1}{r}\sin(B_g r)$ for 1-D slabs, cylinders, and spheres, respectively).

To calculate the coefficient A_1, Eq. (5.21) is substituted into the equation for the POI, Eq. (5.1). The result is then multiplied by R_1 and integrated over the domain, effectively weighting the solution with the spatial profile of the fundamental mode :

$$-B_g^2 A_1 \varrho = -B_m^2 A_1 \varrho + \sum_{j=2}^{J} (-1)^j C_j A_1^j \int_{\vec{r}} R_1^{j+1}(\vec{r}) d\vec{r} \tag{5.23}$$

where :

$$\varrho = \int_{\vec{r}} R_1^2(\vec{r}) d\vec{r} \tag{5.24}$$

Some reorganizing of Eq. (5.23) produces a polynomial whose roots are the coefficient being sought. The root between one and zero is the central value of the fundamental mode approximation of the POI :

$$0 = \rho A_1 - \frac{1}{\varrho \bar{\nu}} \sum_{j=2}^{J} \frac{(-1)^j \chi_j}{j!} A_1^j \int_{\vec{r}} R_1^{j+1}(\vec{r}) d\vec{r} \tag{5.25}$$

5.3 Numerical Results of the Time-Independent Solutions

Definite integrals without a closed form solution, such as those represented in Eq. (5.16), Eq. (5.17), and Eq. (5.19), are evaluated using a Gauss-Kronrod quadrature formula combining a 7-point Gauss rule and a 15-point Kronrod Rule [16]. Unfortunately, some error, $\sim 5 \cdot 10^{-9}$, is introduced by way of the integrable singularity at $y = 1$. Newton-Raphson iteration schemes are considered to have converged if the difference between the value for a given iteration and the one previous is less than $4.4408 \cdot 10^{-16}$.

Because the semi-analytical technique produces a solution requiring no further approximation, it will be examined first to show the actual spatial profile of the POI, shown below in Figure 5.1 for varying values of k_{eff} and J.

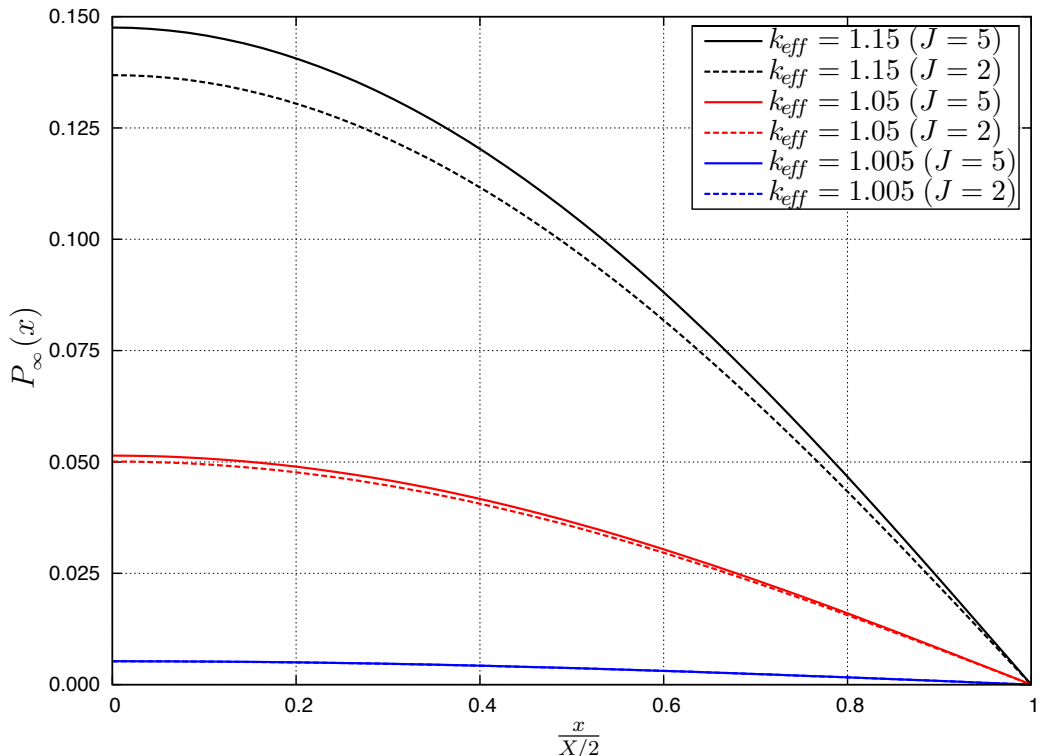

Figure 5.1: P_∞ Throughout a One-Dimensional Slab

The results shown in Figure 5.1 keep well with expectations. As can be seen, the peak magnitude of the POI trends as the excess reactivity of the system, and the spatial profile at least qualitatively resembles that of a corresponding importance function. Also evident is the impact of preserving higher order nonlinearity as a function of the magnitude of the POI.

While it is clear that the contribution of higher order nonlinear terms is felt in the magnitude of the POI, it is not clear from Figure 5.1 how they impact the relative shape. To better understand this impact, the difference between a solution for a given degree of nonlinearity relative to the solution computed for full nonlinearity is plotted in Figure 5.2.

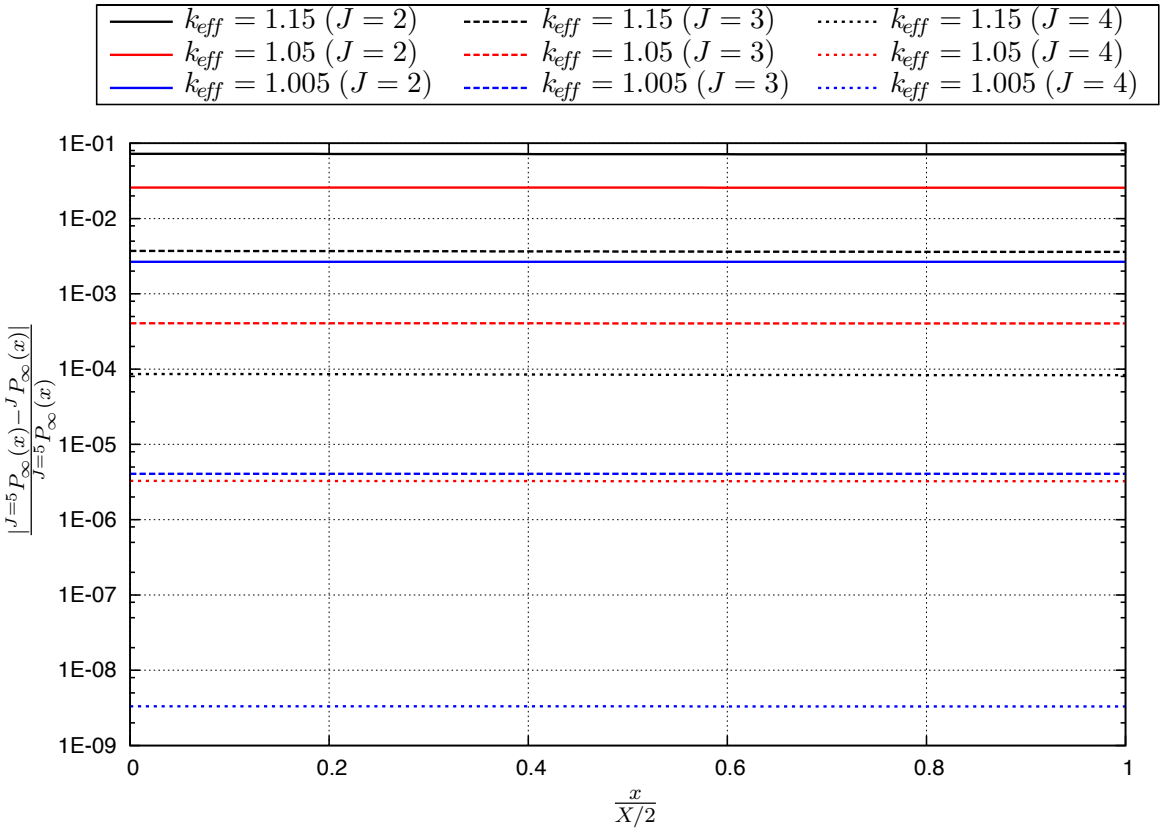

Figure 5.2: Error in P_∞ Relative to the Fully Nonlinear $(J = 5)$ Solution

Figure 5.2 shows that the relative error between solutions corresponding to various values of J is constant throughout the slab. That successive nonlinear terms affect the relative error of the profile uniformly lends strong support to Bell's supposition that the shape of the POI is largely dictated by the linear portion of the equation [4]. Moreover, Figure 5.2 shows that this is so for more than just modest excess reactivities.

With Figure 5.2 clearly demonstrating that the shape of the relative error in the POI is not impacted by varying degrees of nonlinearity for varying values of k_{eff}, Figure 5.3 serves as a complement, showing the impact that preserving additional nonlinear terms has on the magnitude of the POI as a function of k_{eff}.

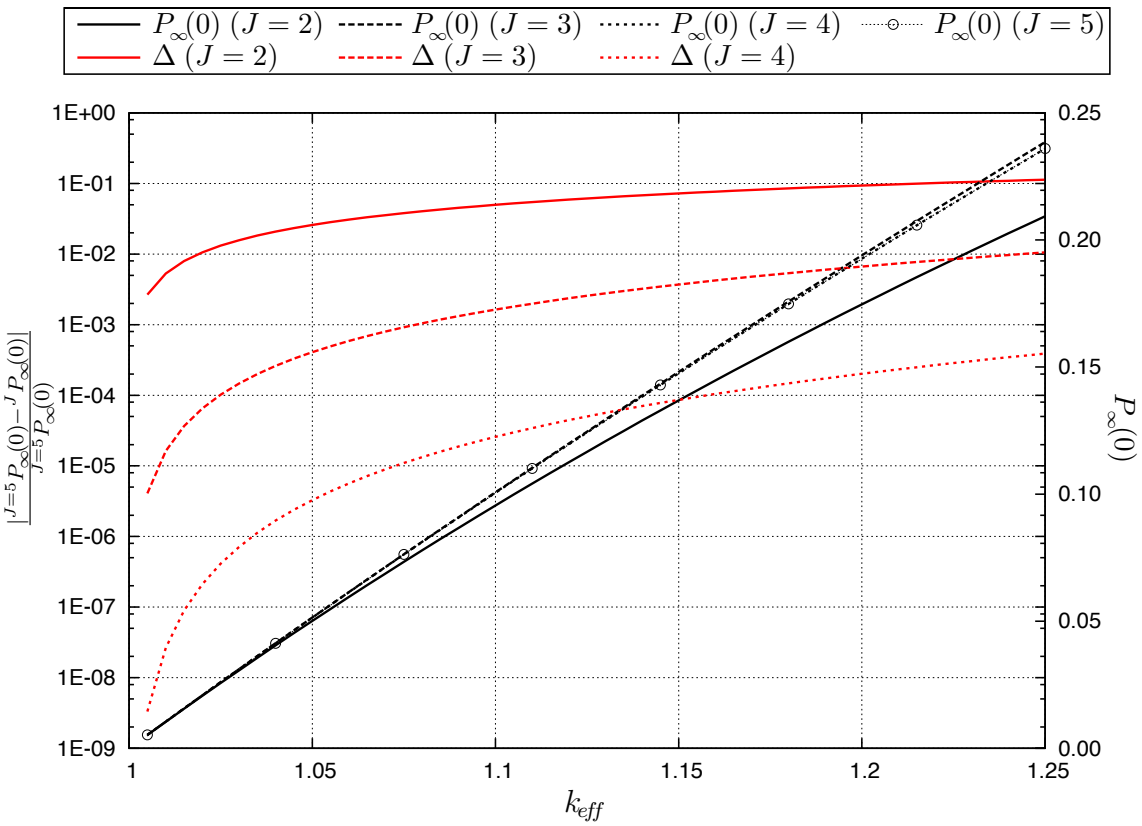

Figure 5.3: $P_\infty(0)$ and Error in $P_\infty(0)$ Relative to the Fully Nonlinear $(J = 5)$ Solution

While the development of the fundamental mode approximation was for general geometries, the results examined here will initially be restricted to those of a one-dimensional slab to permit direct comparison with the semi-analytical solutions. Extension to other geometries is straightforward, accomplished with a simple substitution of the corresponding fundamental mode eigenfunctions, and will be examined later.

A qualitative comparison of the computed semi-analytical survival probability, the corresponding fundamental mode approximation, and the 0-D lumped model solution is made in Figure 5.4.

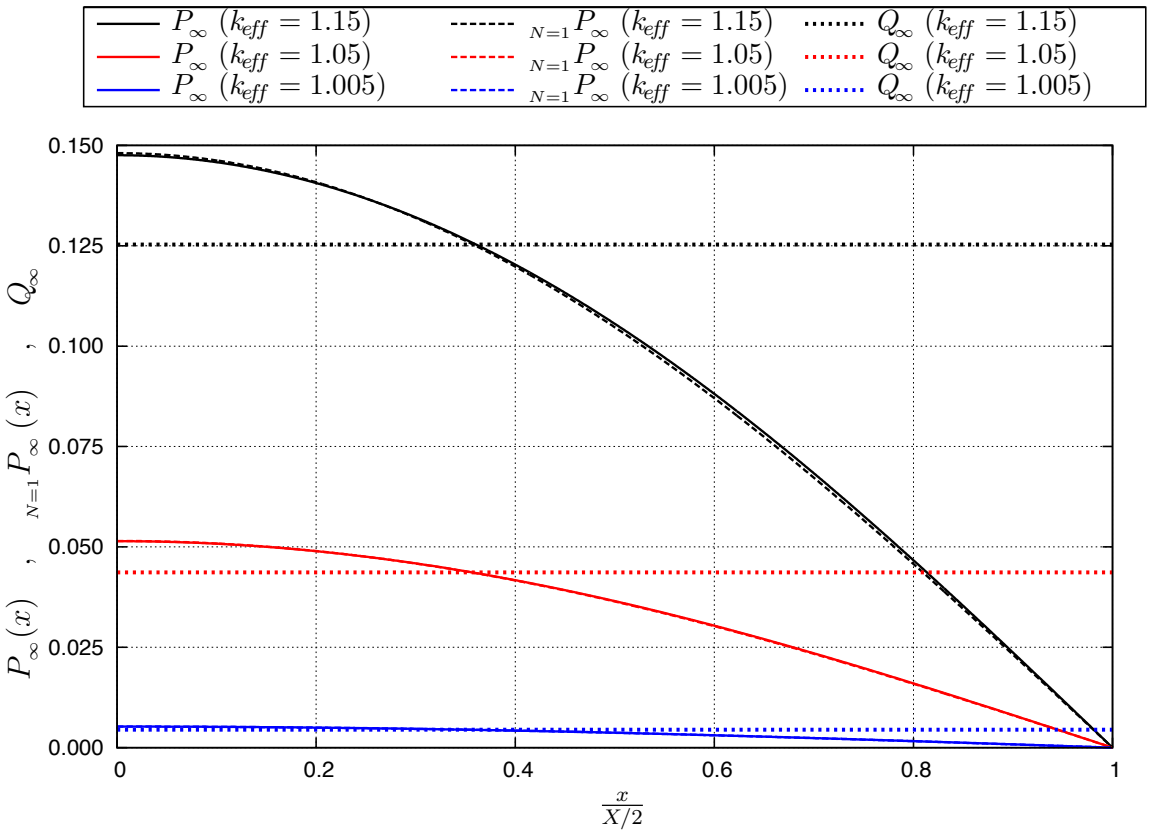

Figure 5.4: P_∞, $_{N=1}P_\infty$, and Q_∞ $(J = 5)$

Figure 5.4 confirms strong qualitative congruence between the semi-analytical POI and its fundamental mode approximation. As expected, distinction between

the two grows as a function of the excess reactivity of the system. While Figure 5.4 only shows results for full nonlinearity, Figure 5.2 showed that the relative shape does not change with varying nonlinearity. It is therefore expected that the fundamental mode approximation should have a similarly constant relative difference in shape. To quantify the magnitude of error introduced by assuming the shape of the POI is described by a fundamental mode approximation, relative and absolute differences for varying degrees of nonlinearity are shown in Figure 5.5.

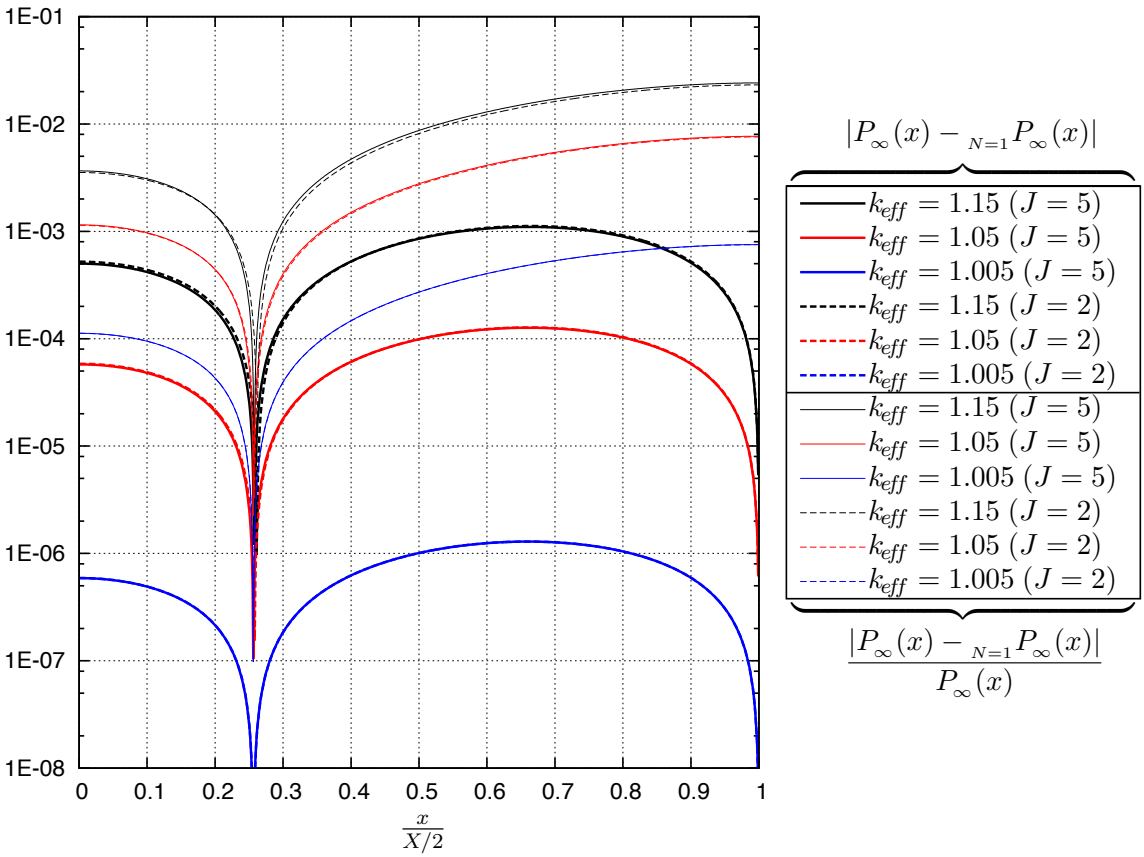

Figure 5.5: Absolute and Relative Differences Between P_∞ and ${}_{N=1}P_\infty$

Figure 5.5 confirms that the fundamental mode approximation works as well as it does for a given k_{eff} regardless of the degree of nonlinearity, as the series for the quadratic and quintic errors are barely distinguishable from one another.

It stands to reason that such an approximation should work so well in spite of the fact that the eigenfunctions are only associated with the linear portion of the equation if the nonlinear fission terms are simply regarded as an arbitrary function of space, representing a source. The equation is then reduced from a nonlinear differential equation to a more common inhomogeneous Helmholtz Equation, whose solutions should be satisfied by the corresponding eigenfunctions.

Having observed that the fundamental mode approximation does so well to represent the POI, and that it renders solutions in geometries accessible where a semi-analytical solution is not, a sense of the difference that changes in geometry have on the steady-state solution can be developed. The fundamental mode approximations for various geometries are plotted below in Figure 5.6.

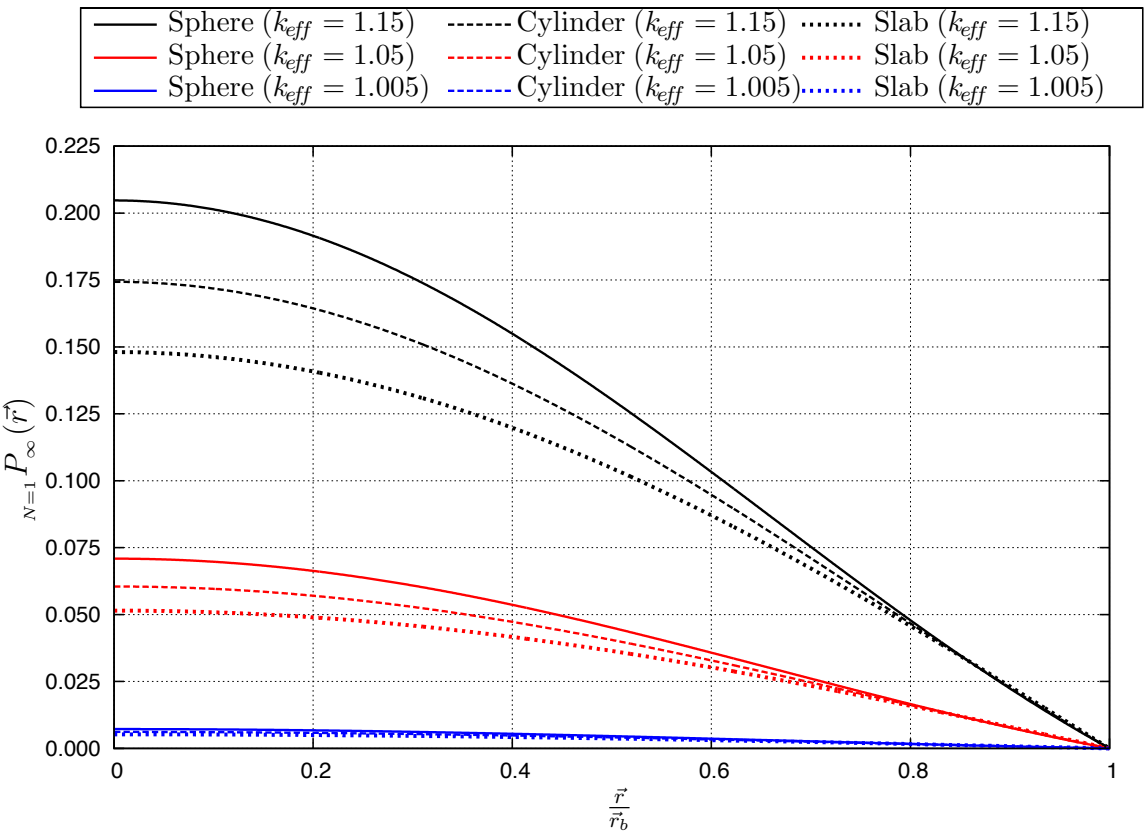

Figure 5.6: $_{N=1}P_{\infty}$ for Various One-Dimensional Geometries ($J = 5$)

As expected, the magnitude of the POI grows with additional dimensional finiteness for a given k_{eff}. This is the case because for a given k_{eff}, a system proliferates particles at a prescribed rate, regardless of geometry. To preserve the system's capacity for particle proliferation with increased dimensional finiteness but constant material properties, the characteristic dimension of a system is increased. Therefore, a particle "injected" at the center of that medium must travel more mean free paths to reach the surface and escape. It follows that the probability of that particle interacting with the medium and causing fission is thereby increased; so too is the probability of initiation. Figure 5.7 demonstrates this through a wide range of k_{eff}.

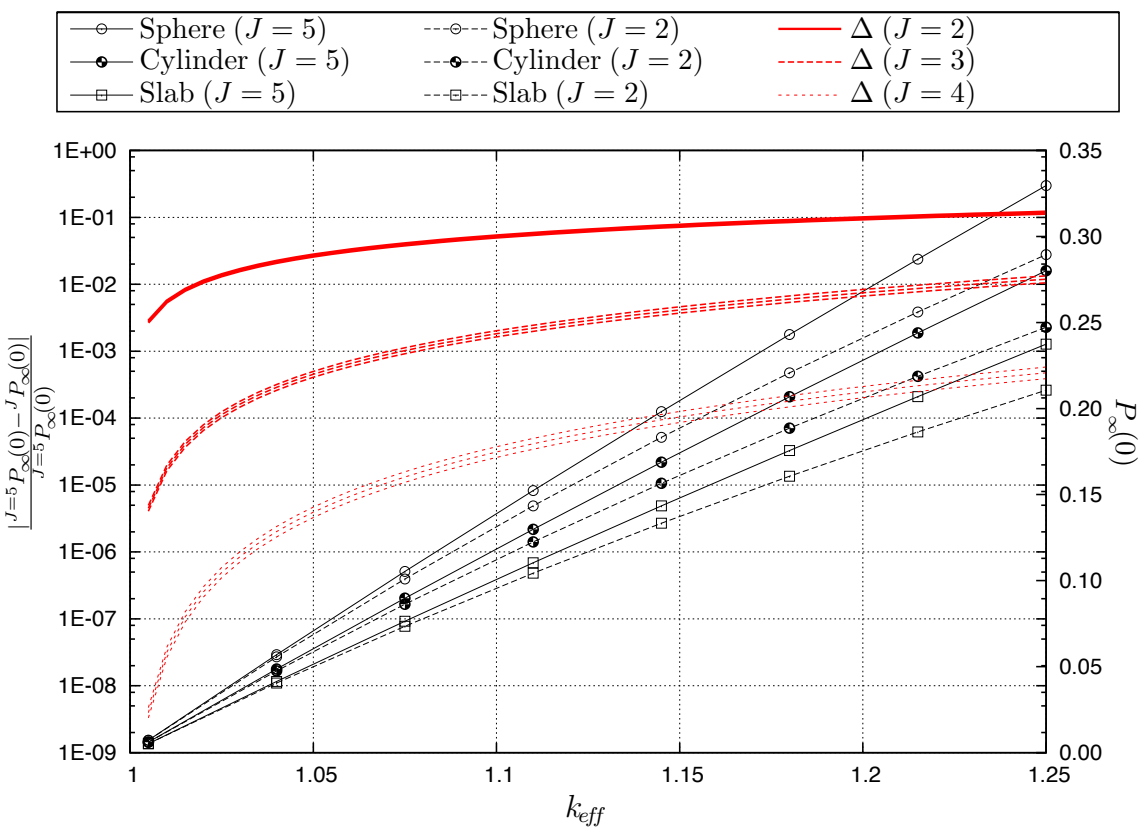

Figure 5.7: $P_\infty(0)$ and Error in $P_\infty(0)$ Relative to the Fully Nonlinear ($J = 5$) Solution in Various One-Dimensional Geometries

In addition to verifying that magnitudes of the survival probability grow with increasing finiteness for a given k_{eff}, Figure 5.7 also shows that the error associated

with truncating nonlinear terms is not particularly sensitive to varying system geometry. Being that no such sensitivity is to be expected, the slight differences that are visible are attributable to the fact that such errors are a function of the magnitude of the POI itself.

5.4 Conclusions from the Space-Dependent POI Solutions

Study of the semi-analytical POI showed the importance of preserving nonlinearity to achieve a given accuracy throughout the medium of interest in much the same way that the results of the spatially uniform lumped model did. As with the results offered by the lumped model, the quadratic approximation was found to produce solutions that underestimate the peak magnitude of the POI by $\sim 10\%$ for values approaching ~ 0.2; while setting $J = 3$ was found to produce solutions with errors of less than 1% for values exceeding ~ 0.2. Again, the accuracy of a solution associated with a given J is dependent on the magnitude of the survival probability.

Additionally, it was demonstrated that the the shape of the relative error in the POI is constant throughout the medium regardless of J, strongly supporting the posit that the shape of the survival probability is defined by the linear portion of the survival probability equation. Comparison to a fundamental mode approximation showed strong agreement, providing direct confirmation that spatial profiles associated with the linear portion of the equation represent the survival probability well, even for high values of k_{eff}, and regardless of J.

Chapter 6

Solution By Eigenfunction Expansion

While the space-dependent steady-state solutions examined in the previous chapter inform a great deal as to the shape that the survival probability takes as it reaches an equilibrium solution, the "initial" condition requires that the survival probability be uniform throughout the medium "initially." Although the 0-D lumped model serves this assumption well, it fails to capture the impact that the spatial variation has on the survival probability when the survival time is nonzero. As was outlined in the introduction, an understanding of the behavior of the time and space-dependent survival probability is desirable.

It was demonstrated that a fundamental mode approximation does remarkably well to represent the POI for even large values of k_{eff}, regardless of the nonlinearity of the equation. Unfortunately, such an approximation will obviously do quite poorly to capture the "initial" condition being that it must be uniform throughout at that point. Being that the eigenfunctions of the linear portion of the survival probability equation are solutions to a Sturm-Liouville problem, it is known that a corresponding

eigenfunction expansion is capable of representing any piecewise smooth function, including a uniform value [17]. Both the "initial" condition and the POI are piecewise smooth, and there is no compelling reason to believe that the survival probability would become otherwise as it evolves through time.

These observations, in concert with an appreciation for the need to be able to preserve arbitrary degrees of nonlinearity, spur the utilization of an eigenfunction expansion technique for solution of the time-dependent survival probability equation.

6.1 Development of an Eigenfunction Expansion Solution Technique

It is first assumed that the survival probability is separable in space and time, and that it may be described by an expansion into a complete set of eigenfunctions :

$$P\left(\vec{r},\tau\right)=\sum_{n=1}^{\infty}T_{n}\left(\tau\right)R_{n}\left(\vec{r}\right) \tag{6.1}$$

In Eq. (6.1) R_n represents the n^{th} eigenfunction and T_n the associated time-dependent coefficient. Substituting the expansion into the survival probability equation leads to an infinite number of linked nonlinear partial differential equations :

$$L^{2}\sum_{n=1}^{\infty}T_{n}\nabla^{2}R_{n}-\sum_{n=1}^{\infty}\frac{\partial T_{n}}{\partial\tau}R_{n}=\left(1-k_{\infty}\right)\sum_{n=1}^{\infty}T_{n}R_{n} + \frac{\Sigma_{F}}{\Sigma_{A}}\sum_{j=2}^{J}\frac{\left(-1\right)^{j}\chi_{j}}{j!}\left[\sum_{n=1}^{\infty}T_{n}R_{n}\right]^{j} \tag{6.2}$$

with the "initial" conditions :

$$\sum_{n=1}^{\infty}T_{n}\left(0\right)R_{n}\left(\vec{r}\right) \quad = \quad 1 \qquad\qquad \vec{r}\in\mathrm{R} \tag{6.3}$$

and the boundary conditions :

$$\sum_{n=1}^{\infty} T_n(\tau) R_n(\vec{r}) \quad = \quad 0 \qquad\qquad \vec{r} \notin \mathrm{R} \tag{6.4}$$

The eigenfunctions of the linear portion of Eq. (6.2) will be used for R_n. That is to say, R_n is the solution to a Sturm-Liouville Equation satisfying the above boundary conditions :

$$\nabla^2 R_n = -\lambda_n^2 R_n \tag{6.5}$$

In addition to providing eigenfunctions for R_n, this allows for the substitution of $-\lambda_n^2 R_n$ in the place of $\nabla^2 R_n$ in Eq. (6.2), reducing the system of partial differential equations to one of ordinary differential equations :

$$-\sum_{n=1}^{\infty} \frac{dT_n}{d\tau} R_n = \sum_{n=1}^{\infty} \left(1 - k_\infty + L^2\lambda_n^2\right) T_n R_n + \frac{\Sigma_F}{\Sigma_A} \sum_{j=2}^{J} \frac{(-1)^j \chi_j}{j!} \left[\sum_{n=1}^{\infty} T_n R_n\right]^j \tag{6.6}$$

Because the eigenfunctions are orthogonal to one another, multiplying Eq. (6.2), by R_m and integrating over $\vec{r}$ removes the dependence on $\vec{r}$:

$$\begin{aligned} -\int_{\vec{r}} \sum_{n=1}^{\infty} \frac{dT_n}{d\tau} R_n R_m d\vec{r} = & \int_{\vec{r}} \sum_{n=1}^{\infty} \left(1 - k_\infty + L^2\lambda_n^2\right) T_n R_n R_m d\vec{r} \\ & + \frac{\Sigma_F}{\Sigma_A} \sum_{j=2}^{J} \frac{(-1)^j \chi_j}{j!} \int_{\vec{r}} \left[\sum_{n=1}^{\infty} T_n R_n\right]^j R_m d\vec{r} \end{aligned}$$

$$\frac{dT_m}{d\tau} = \left(k_\infty - 1 - L^2\lambda_m^2\right) T_m - \frac{\Sigma_F}{\Sigma_A \varrho_m} \sum_{j=2}^{J} \frac{(-1)^j \chi_j}{j!} \int_{\vec{r}} R_m \left[\sum_{n=1}^{\infty} T_n R_n\right]^j d\vec{r} \tag{6.7}$$

where advantage has been taken of :

$$\int_{\vec{r}} R_n R_m d\vec{r} = \varrho_m \delta_{nm} \tag{6.8}$$

To compute the "initial" conditions for the differential equations represented by Eq. (6.7), the orthogonality of the eigenfunctions is again exploited by multiplying Eq. (6.3) by R_m and integrating over $\vec{r}$:

$$\int_{\vec{r}} \sum_{n=1}^{\infty} T_n(0) R_n R_m d\vec{r} = \int_{\vec{r}} R_m d\vec{r}$$

$$T_m(0) = \frac{1}{\varrho_m} \int_{\vec{r}} R_m d\vec{r} \tag{6.9}$$

Where as invoking the orthogonality of the eigenfunctions normally produces a series of decoupled differential equations, Eq. (6.7) represents an infinite set of linked nonlinear differential equations. The solutions are the temporal coefficients of the eigenfunctions of the survival probability. If a solution to such a set of differential equations is to be had, the eigenfunction expansion must be truncated to a finite number of modes, N :

$$\frac{dT_m}{d\tau} = \left(k_\infty - 1 - L^2\lambda_n^2\right) T_m - \frac{\Sigma_F}{\Sigma_A \varrho_m} \sum_{j=2}^{J} \frac{(-1)^j \chi_j}{j!} \int_{\vec{r}} R_m \left[\sum_{n=1}^{N} T_n R_n\right]^j d\vec{r} \tag{6.10}$$

Owing to the nonlinearity of the survival probability equation, computing the coefficients of the nonlinear terms in Eq. (6.10) becomes increasingly laborious for larger expansions. Setting the derivative with respect to time equal to zero results in a set of N linked polynomials where the coefficients that satisfy the set of equations are those associated with the eigenfunctions that define the POI. These solutions can serve as a means to compute the POI more rapidly, if that is all that is desired, as well as a means to ensure that the time-dependent solver converges correctly.

6.1.1 Diffusion Approximation Eigenfunctions

As previously mentioned, the diffusion approximation is applied here not only to enjoy the simplicity afforded by removing the dependence of the survival probability

on angle, but also so that the exact eigenfunctions of the resulting equation for special geometries may be exploited. Doing so allows for the efficacy of solution by eigenfunction expansion to be examined without having to expend additional effort computing eigenfunctions to begin with.

Because solutions to the Helmholtz equation with homogeneous boundary conditions are well understood for general geometries (e.g., slabs, cylinders, and spheres), they will simply be reproduced here for completeness.

Table 6.1: Eigenfunctions and Geometric Buckling

Geometry	Eigenfunction (R_n)	Geometric Buckling (B_g^2)
1-D Slab	$\cos\left(\frac{(2n-1)\,\pi}{X}x\right)$	$\left(\frac{\pi}{X}\right)^2$
1-D Cylinder	$\mathrm{J}_0\left(\frac{j_n}{R}r\right)$	$\left(\frac{j_1}{R}\right)^2$
Sphere	$\frac{1}{r}\sin\left(\frac{n\pi}{R}r\right)$	$\left(\frac{\pi}{R}\right)^2$
2-D Slab	$\cos\left(\frac{(2a-1)\,\pi}{X}x\right)\cos\left(\frac{(2b-1)\,\pi}{Y}y\right)$	$\left(\frac{\pi}{X}\right)^2+\left(\frac{\pi}{Y}\right)^2$

Here, J_0 is a Bessel function of the first kind and j_n is the n^{th} zero of that function, which are computed using Halley's method [18].

System dimensions (i.e., slab side lengths X and Y, and cylindrical and spherical radii R) are computed for a given geometry and k_{eff} in the usual way by equating the geometry dependent definition of the geometric buckling from Table 6.1, which results from the relevant boundary conditions, to the general definition of geometric buckling, B_g^2 :

$$B_g^2 = \frac{\frac{k_\infty}{k_{eff}} - 1}{L^2} \tag{6.11}$$

6.1.2 Applying the Quadratic and Fundamental Mode Approximations : Development of an Analytical Expression for a Time and Space-Dependent Lumped Model

As with the 0-D lumped model, applying the quadratic approximation permits an analytical expression for the survival probability if the fundamental mode approximation is also applied. Such an expression can be viewed as a time and space-dependent lumped model, affording an extremely computationally economical solution.

Unfortunately, this analytical expression is only available if these approximations are applied, so it is therefore subject to the same significant errors for large survival probabilities. Despite these shortcomings, Eq. (6.12) requires next to nothing computationally, being that it is an analytical expression, and can serve well depending on the level of accuracy needed. Additionally, it provides a benchmark against which the ability of a numerical scheme to handle the stiffness of the survival probability equation may be measured.

Following the development presented in Chapter 3 for the 0-D lumped model as applied to Eq. (6.10) for an unimodal "expansion" (i.e., $J = 2$ and $N = 1$) :

$$_{N=1}P\left(\vec{r},\tau\right) = \frac{R_1\left(\vec{r}\right)}{\frac{\beta}{\alpha} + \left(\frac{\varrho_1}{\int_{\vec{r}} R_1 d\vec{r}} - \frac{\beta}{\alpha}\right) e^{-\alpha\tau}} \tag{6.12}$$

where :

$$\alpha = \left(k_\infty - 1 - L^2\lambda_1^2\right) \tag{6.13}$$

$$\beta = \frac{\Sigma_F}{\varrho_1 \Sigma_A} \frac{\chi_2}{2!} \int_{\vec{r}} R_1^3 d\vec{r} \tag{6.14}$$

6.2 Benchmarking the EFE Technique : Numerical Results in a 1-D Slab

The present focus will be restricted to the simple case of a one-dimensional slab so that solutions provided by the eigenfunction expansion may be compared against the benchmark provided by the semi-analytical POI developed in Chapter 5. Extension to other geometries is straightforward, and is deferred to a later point so as not to becloud that which we wish to examine.

Because the Helmholtz equation from which the eigenfunctions were derived is a Sturm-Liouville problem, it is known that as N goes to infinity, the expansion representation is able to converge exactly on the spatially uniform "initial" condition, for it is a smooth function. Figure 6.1 shows this convergence for increasing N.

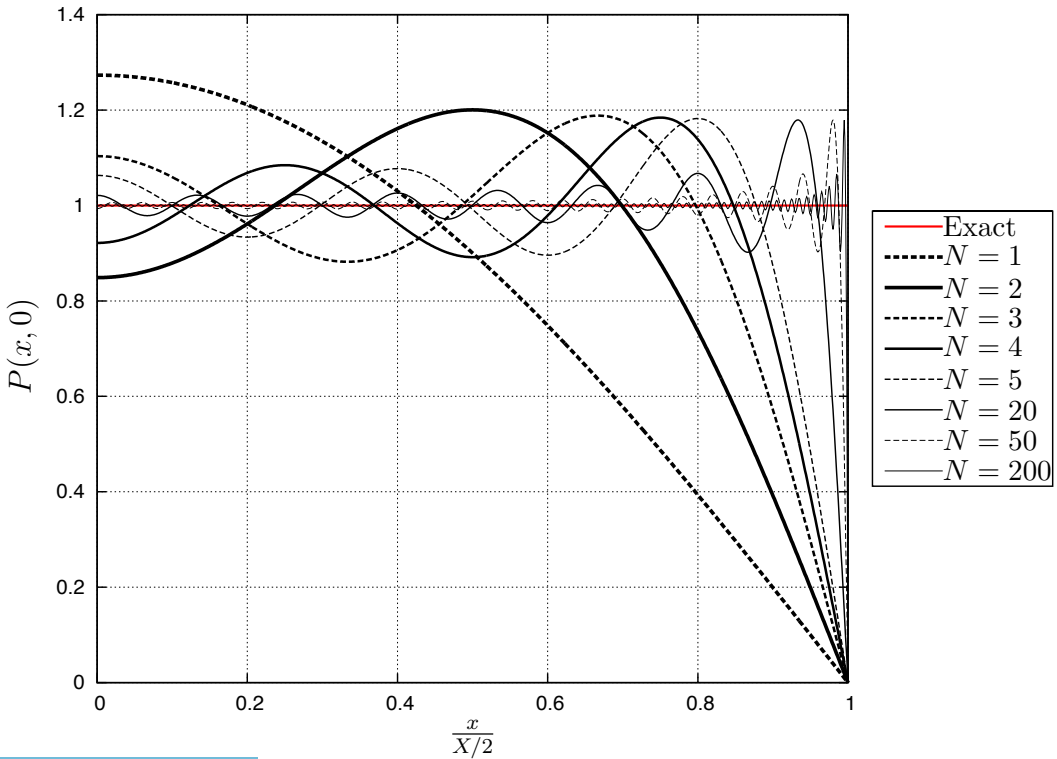

Figure 6.1: Eigenfunction Expansion "Initial" Condition for Varying N

It was shown in Chapter 5 that the fundamental mode approximation did quite well to represent the POI, in part spurring the use of the eigenfunction expansion technique here to determine whether or not additional modes could provide for a more accurate solution. Figure 6.2 below provides a qualitative confirmation that they indeed can.

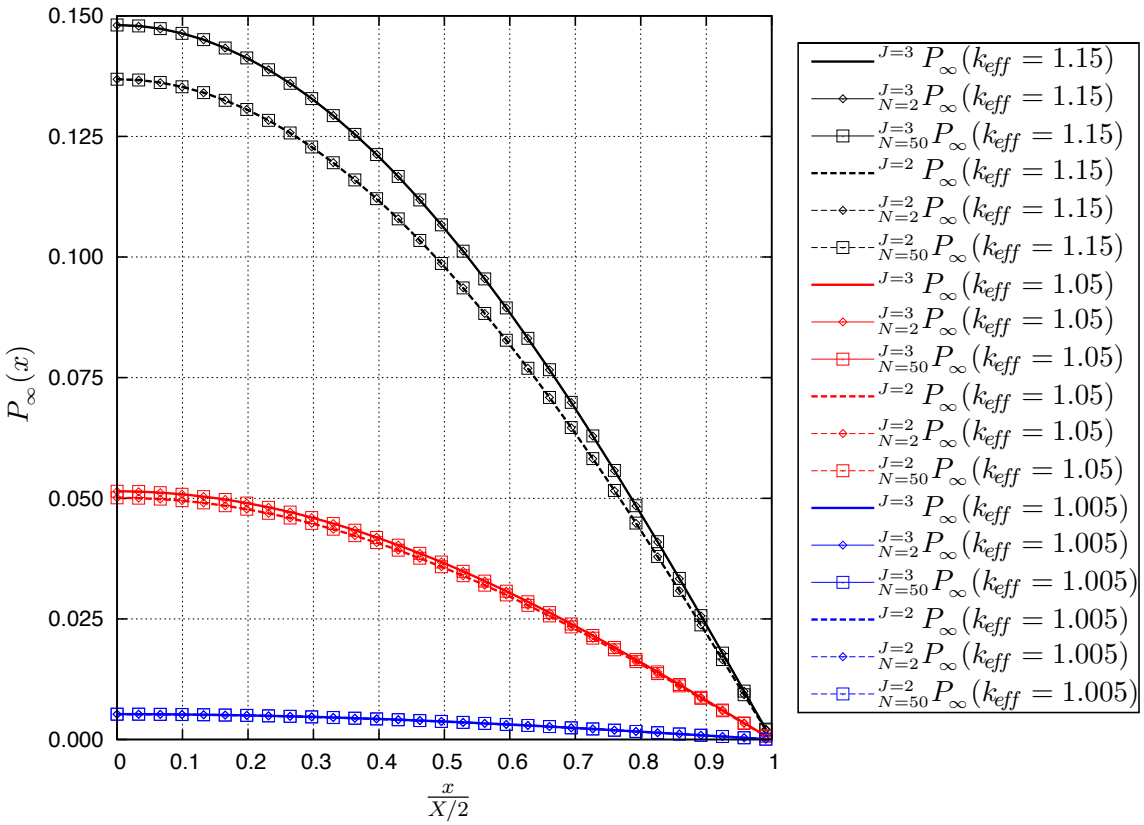

Figure 6.2: Semi-Analytical P_∞ and EFE ${}_N P_\infty$ for Varying k_{eff}, J, and N

Figure 6.2 shows that regardless of k_{eff} or J, the addition of even just one mode beyond the fundamental brings the computed POI much closer to the semi-analytical solution. The difference between the semi-analytical solutions and those for two and fifty mode expansions is not discernible in the above plot throughout the parameter space. To quantify the impact that additional modes has on the solution accuracy, the maximum error that exists within the slab is plotted as a function of N in Figure

6.3

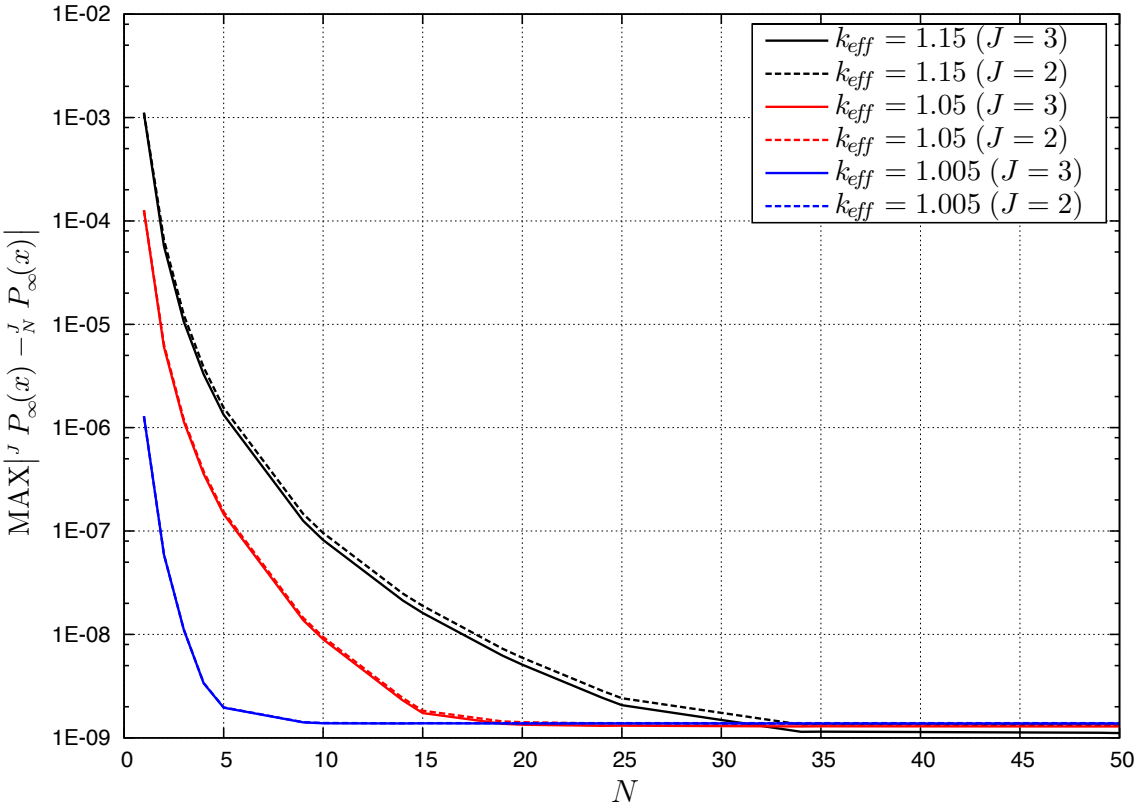

Figure 6.3: Maximum Difference Within Slab Between Semi-Analytical P_∞ and EFE P_∞ for Varying k_{eff}, J, and N

Figure 6.3 demonstrates the expected EFE solution accuracy increase with increasing N, ultimately converging on the upper limit of accuracy afforded in the semi-analytical solution. It also shows that for smaller values of the POI, fewer modes are needed to achieve a given accuracy. This stands to reason, for as k_{eff} increases toward k_∞, the shape of the POI goes from a shape that is very well represented by the corresponding fundamental mode approximation toward a uniform value. As Figure 6.1 shows, more modes are needed to accurately represent profiles that are more spatially uniform.

For the steady-state case, that the accuracy of a given expansion as a function of N is only indirectly coupled with the values of J and k_{eff}, in that they inform the magnitude of the POI, is consistent with the comparison of the semi-analytical and fundamental mode approximation POIs.

Figures 6.1 through 6.3 demonstrate the ability of the EFE technique to accurately produce the survival probability at both the "initial" and equilibrium states for varying k_{eff} and J. While these are the only two points for which an analytical solution is available for direct comparison, confidence in the ability of the technique, as well as the numerical routine, is bolstered by consistency in comparison with the existing developed analytical expressions as well :

- Setting the derivative with respect to time in Eq. (6.10) to zero and solving the resultant system of steady-state equations produces coefficients that correspond to an eigenfunction expansion of the POI. For the entire parameter space, these POI values match those that the time-dependent solver converges on.

- The results of the EFE technique with $J = 2$ and $N = 1$ exactly match those produced by the analytical expression developed in Section 6.1.2.

Being that the results are indistinguishable to within the specified precision, there is a high level of confidence in the ability of the technique to solve the stiff differential equations of the eigenfunction expansion and for the convergence criteria to bring about accurate POIs. In other words, given all available benchmarking, the EFE technique proves to be an effective method of solution for survival probability equations of arbitrary nonlinearity.

6.3 Further Examination of the EFE Technique in a 1-D Slab

Because of the additional computational burden of solving higher modal expansions, particularly for higher degrees of nonlinearity, it is important to understand how the accuracy associated with an N-mode expansion varies within the available parameter space. Having examined its accuracy at both the "initial" and equilibrium states, attention will now be directed toward how well an expansion represents the survival probability for varying survival times. As Figure 6.4 shows, the survival probability shifts from its uniform "initial" state to a shape not drastically different than that of a simple fundamental mode after just a single neutron lifetime has passed.

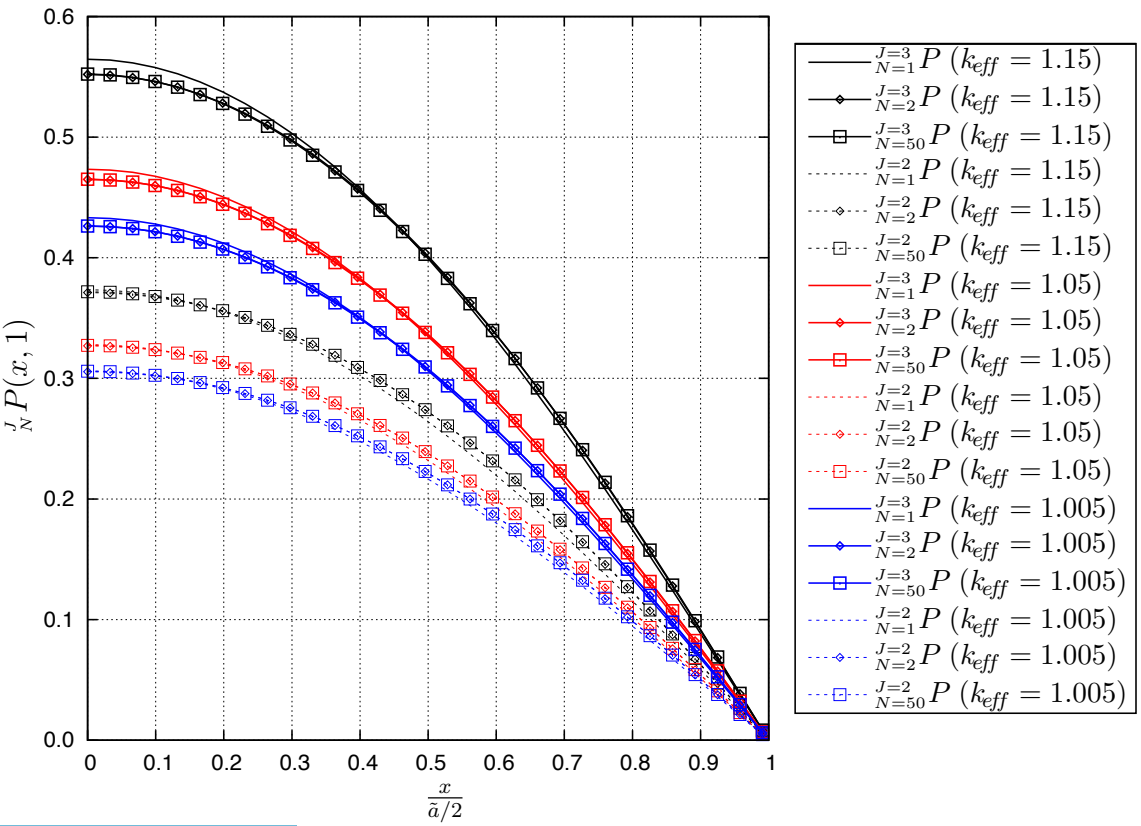

Figure 6.4: P at $\tau = 1$ for Varying k_{eff}, J, and N

Just as with the POIs for higher values of k_{eff}, there is some visible difference between the single mode approximations and multi-mode approximations, yet precious little between various multi-mode approximations. Much more visible is the error associated with truncation of the equation nonlinearity, which overshadows any error associated with modal truncation of the eigenfunction expansion.

To better quantify the impact that increasing N has, the maximum relative error between solutions for varying N will be examined. Unfortunately, there are no available analytical solutions against which the EFE solutions may be measured. Given, however, the known ability of the EFE to accurately represent the "initial" condition with increasing N, and the demonstrated ability to represent the equilibrium state, it is assumed that it does well to model interim solutions as well.

In the absence of an analytical solution, the solution associated with the highest value of N examined, N_{MAX}, is taken to be the most accurate. Therefore, any errors computed ought be relative to those solutions. Computing relative error in the usual way, however, will not provide very insightful information, as convergence on that solution is assured with increasing N. How well a given N mode expansion represents the N_{MAX} mode expansion is not terribly interesting as it does not inform as to the level of convergence on the actual survival probability, because no such value is available.

Operating under the assumption that increasing N increases accuracy, a more valuable measure of the benefit associated with including additional modes in an expansion is how much increasing N alters the solution. Hence, the best measure of the accuracy associated with increasing N as a function of N is given by what will here be called the relative modal error, Δ_N :

$$\Delta_N(\vec{r},\tau) = \frac{|_{N-1}P(\vec{r},\tau) -_N P(\vec{r},\tau)|}{_{N_{MAX}}P(\vec{r},\tau)} \tag{6.15}$$

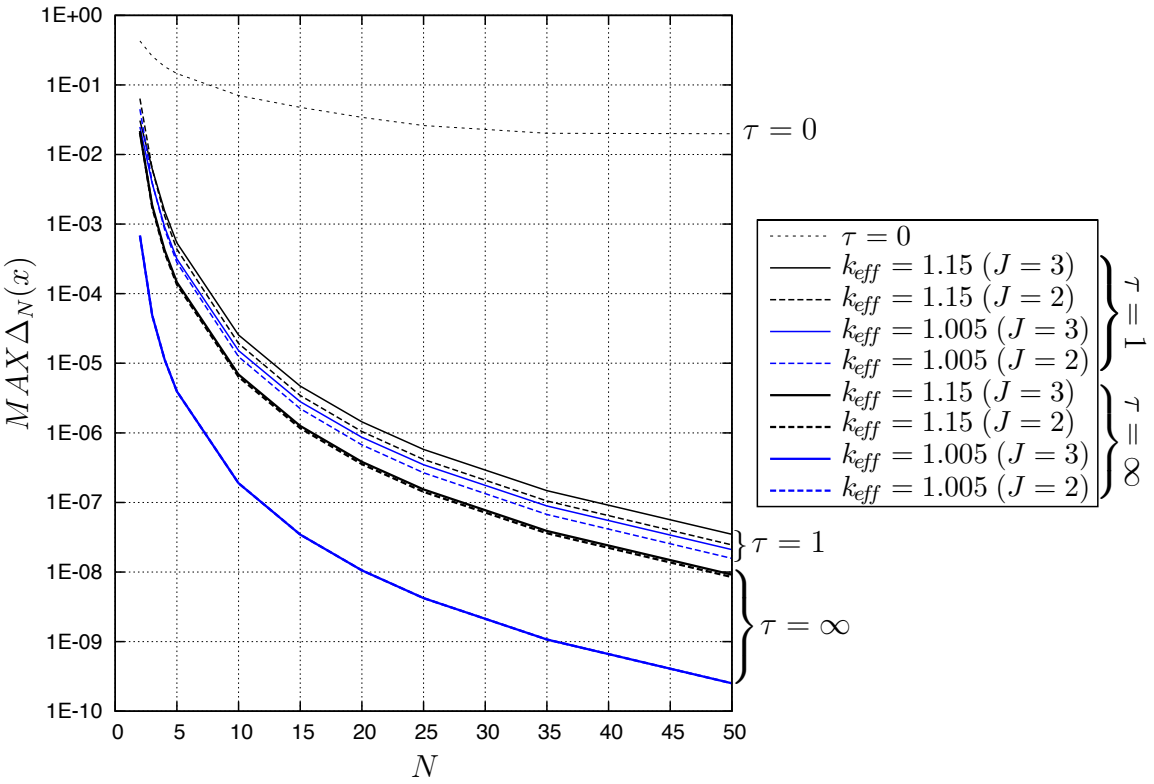

Figure 6.5: Maximum Relative Modal Error in P for Varying τ, k_{eff}, J, and N

Figures 6.3 through 6.5 reinforce that the impact that increasing the number of modes in an expansion has on solution accuracy is only indirectly coupled to τ, k_{eff}, and J by virtue of being directly tied to the magnitude of the survival probability and its departure from its "initial" state. Figure 6.4 shows the shape and magnitude of the survival probability to dramatically change from its "initial" uniform value to one of significantly reduced magnitude, qualitatively resembling a fundamental mode approximation. Figure 6.5 shows the corresponding plummet in relative modal error.

Because the shape and magnitude of the survival probability varies dramatically in early survival times, and less so thereafter, so does the accuracy afforded by an increase in N. To better appreciate the difference that additional modes has for very small survival times, the survival probability within a one-dimensional slab for $N = 2$ and $N = 50$ inside of one neutron lifetime is plotted in Figure 6.6.

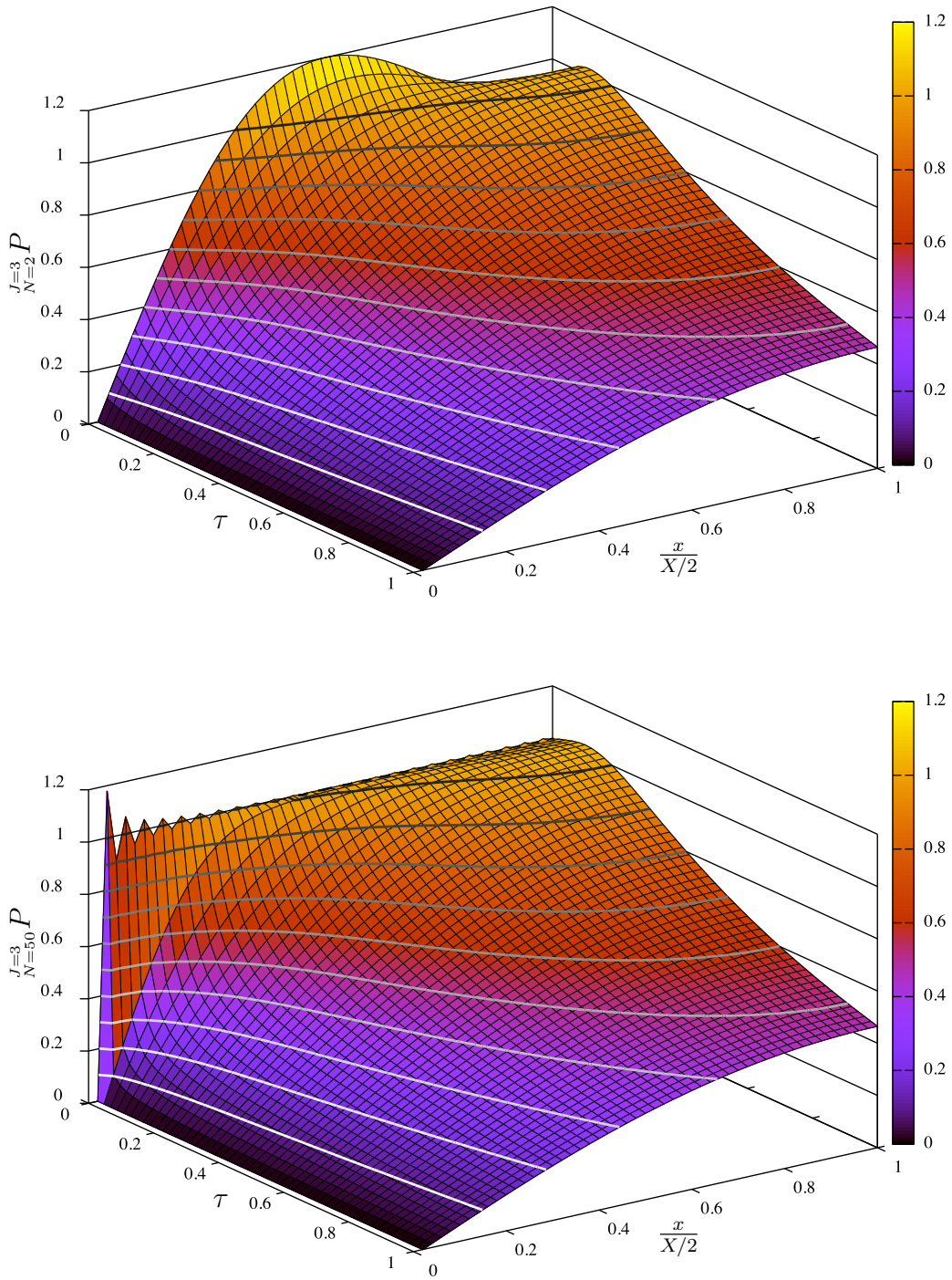

Figure 6.6: $_{N=2}P$ & $_{N=50}P$ in a 1-D Slab for $\tau < 1$ ($k_{eff} = 1.05$ & $J = 3$)

The corresponding maximum relative modal error is plotted below in Figure 6.7.

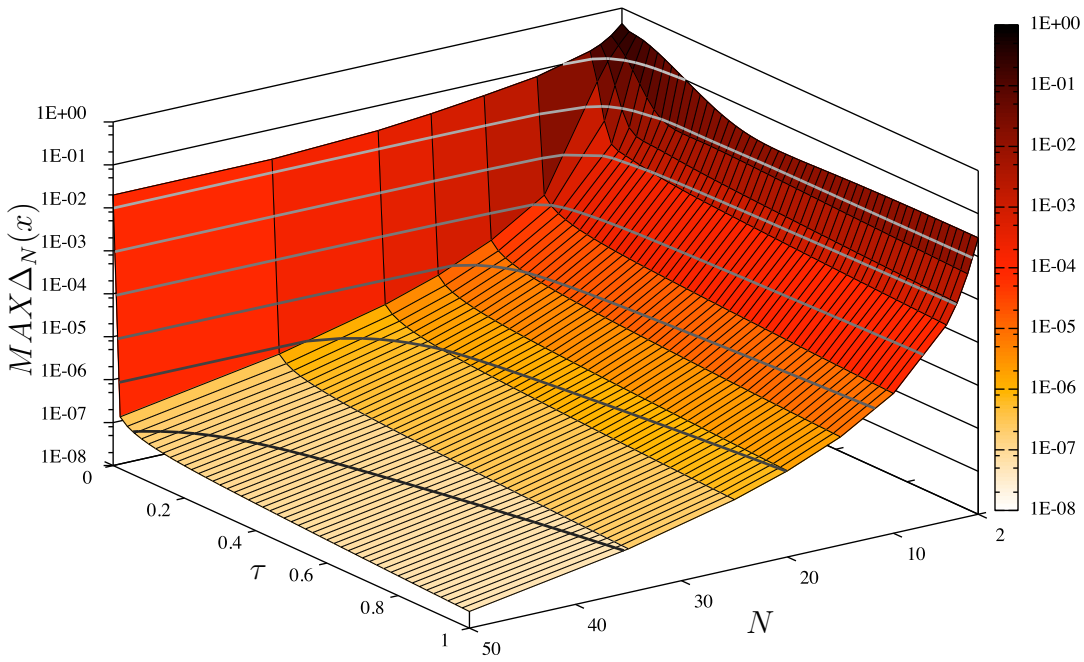

Figure 6.7: Maximum Δ_N for $\tau < 1$ ($k_{eff} = 1.05$ & $N = 3$)

Figure 6.7 makes clear how quickly the accuracy afforded per mode is had with the passage of even a very slight amount of survival time. Even just a ten mode expansion achieves maximum relative modal error of less than two one-hundredths of a percent within the first one-fiftieth of a neutron lifetime.

6.4 Examination of the EFE Technique in Various 1-D Geometries

With a thorough understanding of the ability of the EFE technique to provide solutions throughout the parameter space in a one-dimensional slab, all that remains to be seen is the impact that a change in geometry has on its efficacy. Based on

the results shown for the steady-state case, it is expected that increased finiteness will increase the peak magnitude of the survival probability for a given k_{eff} in the time-dependent case as well. Figure 6.8 confirms that this is so.

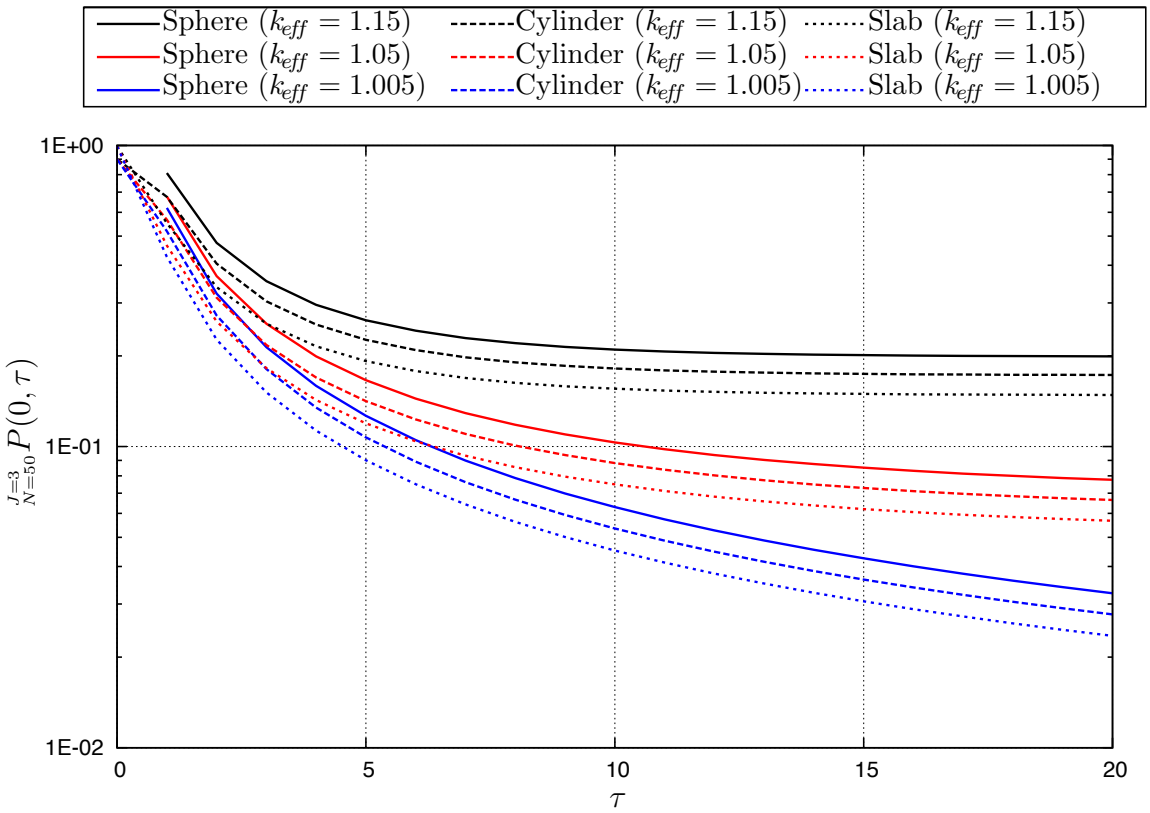

Figure 6.8: $\frac{J=3}{N=50}P(0,\tau)$ in Various Geometries for Small Survival Times ($\tau \leq 20$)

Because of the nature of the eigenfunctions for the spherical geometry, the value at the center alternates between 0 and 2, "initially," for even and odd values of N, respectively. This accounts for the absence of a 0^{th} data point for the spherical cases depicted in Figure 6.8.

While Figure 6.8 gives a sense of the behavior of the survival probability in various geometries, it doesn't show the difference that varying geometry has on the efficacy of the EFE technique. Because there is not an available analytical or semi-analytical solution available for geometries other than a one-dimensional slab, this impact is

only quantifiable by way of the relative modal error. Again, having established that the accuracy of a given truncation is a function of the magnitude of the survival probability, the parameter space will be limited so as to make clear the impact that a change in geometry has.

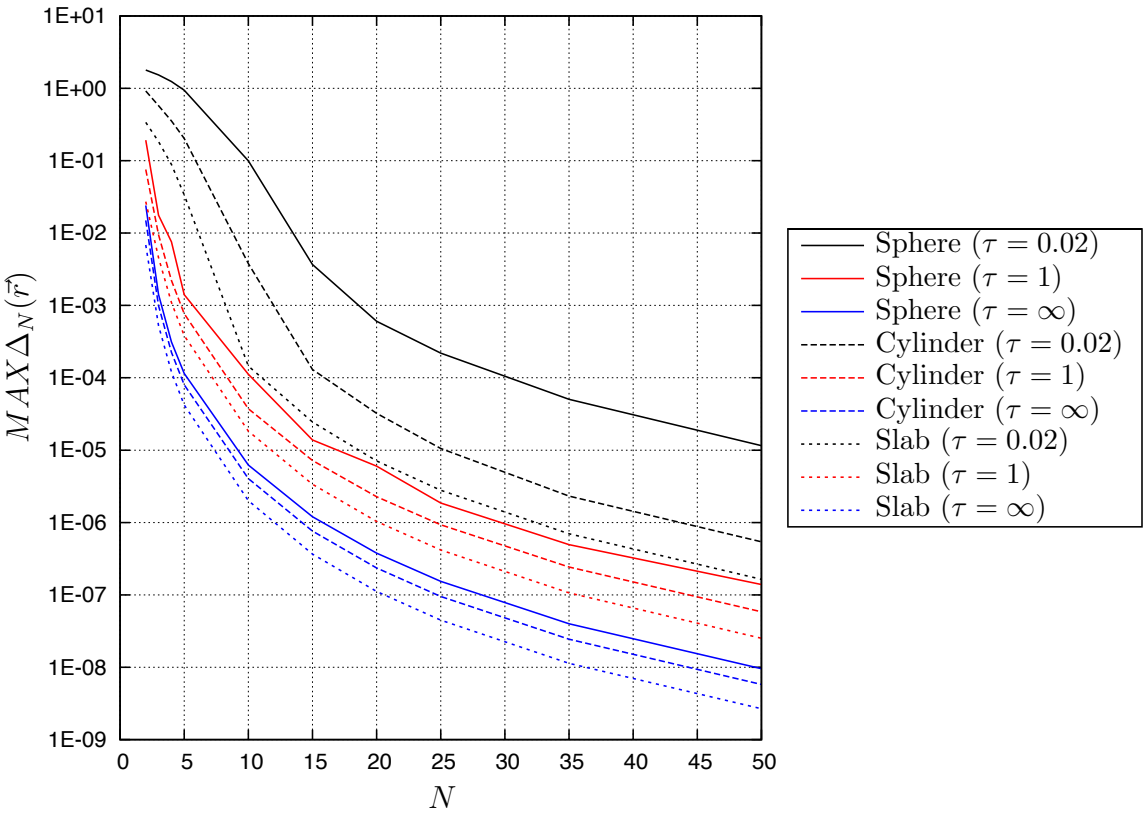

Figure 6.9: Maximum Relative Modal Error in P for Varying τ, N, and Geometry ($k_{eff} = 1.05$ & $J = 3$)

Figure 6.9 does not show the accuracy of a given EFE to be impacted by a change of geometry in any special way. Apparently, as was revealed by the study of the fundamental mode approximations of the POIs for various geometries, the system geometry impacts the accuracy of the eigenfunction expansion approximation in much the same way that τ, k_{eff}, and J do. That is, geometry impacts the accuracy of the EFE by driving the shape and magnitude of the survival probability; the accuracy of a given EFE is a function of the magnitude of the survival probability.

Regardless of geometry, as k_{eff} grows and τ approaches zero, the survival probability grows in magnitude and tends to become more uniform, thereby requiring more modes in an expansion to achieve a given accuracy.

Figure 6.10 shows that a change in system geometry has no dramatic impact on the survival time required to settle on the POI, τ_∞, with the exception of the change from an infinite medium to finite geometries, which roughly halves τ_∞ for a given k_{eff}. Though not depicted below, τ_∞ is not a significant function of N. Again, the nature of the variable order solver used here masks what could only be subtle differences (e.g., a few neutron lifetimes).

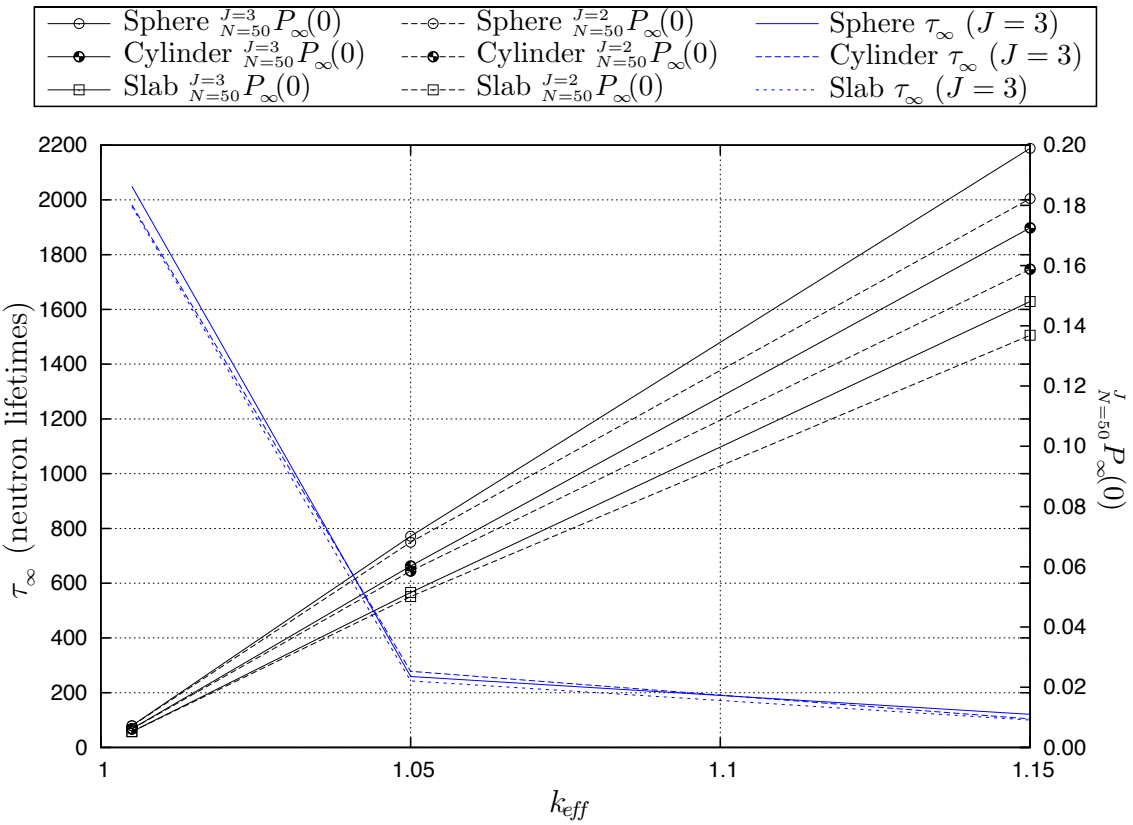

Figure 6.10: $P_\infty(0)$ and τ_∞ for Varying Geometry and k_{eff} $(N = 50)$

6.5 Examination of the EFE Technique in Multi-Dimensional Geometries

While the development of the EFE technique in Section 6.1 was for general geometries, and therefore directly applicable to multi-dimensional geometries as well, the simplicity of the development in a general geometry masks additional complexity brought on by extension to multi-dimensional problems. It's worth exploring these complexities and understanding the impact that they have on solutions.

In the multi-dimensional case, the eigenfunctions of the Helmholtz Equation, Eq. (6.2), are products of eigenfunctions in each of the dimensions, as opposed to individual eigenfunctions as with the 1-D case. As a consequence, the multi-dimensional example of Eq. (6.2), taken out of its expression in general geometry and put into an expression in explicit terms of the relevant dimensions, gains an additional summation per term, per dimension. Although straightforward, extension to higher dimensional geometries does bring with it some complication in procedure. For ease of demonstration, a 2-D slab with lengths X and Y will be examined here.

Again, it is first assumed that the survival probability is separable in space and time. In this case, however, there is an expansion in each dimension :

$$P(x,y,\tau) = \sum_{a=1}^{A} T_a(\tau) R_a(x) \sum_{b=1}^{B} T_b(\tau) R_b(y) \tag{6.16}$$

Here, the expansions are already taken to be finite. As with the general case, Eq. (6.16) is substituted into the survival probability equation :

$$\begin{aligned} -\sum_{a=1}^{A}\sum_{b=1}^{B} \frac{dT_a T_b}{d\tau} R_a R_b = &\sum_{a=1}^{A}\sum_{b=1}^{B} \left(1 - k_\infty + L^2\left[\lambda_a^2 + \lambda_b^2\right]\right) T_a T_b R_a R_b \\ &+ \frac{\Sigma_F}{\Sigma_A} \sum_{j=2}^{J} \frac{(-1)^j \chi_j}{j!} \left[\sum_{a=1}^{A}\sum_{b=1}^{B} T_a T_b R_a R_b\right]^j \end{aligned} \tag{6.17}$$

Because eigenfunctions in each dimension are orthogonal to one another, multiplying Eq. (6.2), by $R_c(x)$ and $R_d(y)$ and integrating over X and Y removes the dependence on x and y. Because T_a and T_b are simply temporal coefficients of the eigenfunctions R_a and R_b, respectively, they may be combined so that Eq. (6.17) becomes a single nonlinear ordinary differential equation, as the EFE technique requires regardless of geometry :

$$
\begin{aligned}
-\int_{-X/2}^{X/2}\int_{-Y/2}^{Y/2}\sum_{a=1}^{A}\sum_{b=1}^{B}\frac{dT_{ab}}{d\tau}R_aR_bR_cR_ddydx = \\
\int_{-X/2}^{X/2}\int_{-Y/2}^{Y/2}\sum_{a=1}^{A}\sum_{b=1}^{B}\left(1-k_\infty+L^2\left[\lambda_a^2+\lambda_b^2\right]\right)T_{ab}R_aR_bR_cR_ddydx \\
+\frac{\Sigma_F}{\Sigma_A}\sum_{j=2}^{J}\frac{(-1)^j\chi_j}{j!}\int_{-X/2}^{X/2}\int_{-Y/2}^{Y/2}\left[\sum_{a=1}^{A}\sum_{b=1}^{B}T_{ab}R_aR_b\right]^j R_cR_ddydx
\end{aligned}
$$

$$
\begin{aligned}
\frac{dT_{cd}}{d\tau} =&\left(k_\infty-1-L^2\left[\lambda_c^2+\lambda_d^2\right]\right)T_{cd} \\
&-\frac{\Sigma_F}{\Sigma_A\varrho_{cd}}\sum_{j=2}^{J}\frac{(-1)^j\chi_j}{j!}\int_{-X/2}^{X/2}\int_{-Y/2}^{Y/2}\left[\sum_{a=1}^{A}\sum_{b=1}^{B}T_{ab}R_aR_b\right]^j R_cR_ddydx
\end{aligned}
\tag{6.18}
$$

where :

$$
\varrho_{cd}=\int_{-X/2}^{X/2}R_c^2dx\int_{-Y/2}^{Y/2}R_d^2dy \tag{6.19}
$$

Eq. (6.18) makes clear the additional computational burden drawn by such a system of equations when expansions grow in each dimension as the number of terms that must be solved for grows as the product of the two raised to whatever degree of nonlinearity being solved for.

While there is no expectation that the essential characteristics of the EFE technique will be drastically affected by this extension, an understanding of the impact that the additional complexity has on the solution behavior is in order.

Bringing to bear the understanding garnered from the examination of the 1-D geometries, plus the understanding that the coefficients of modes in each dimension are intertwined by virtue of effectively sharing with the modes in the other dimension, the plot of a centered cross-section of the "initial" condition in Figure 6.11 exhibits both the expected convergence with an increasing number of modes and the expected enhanced oscillations about the actual value.

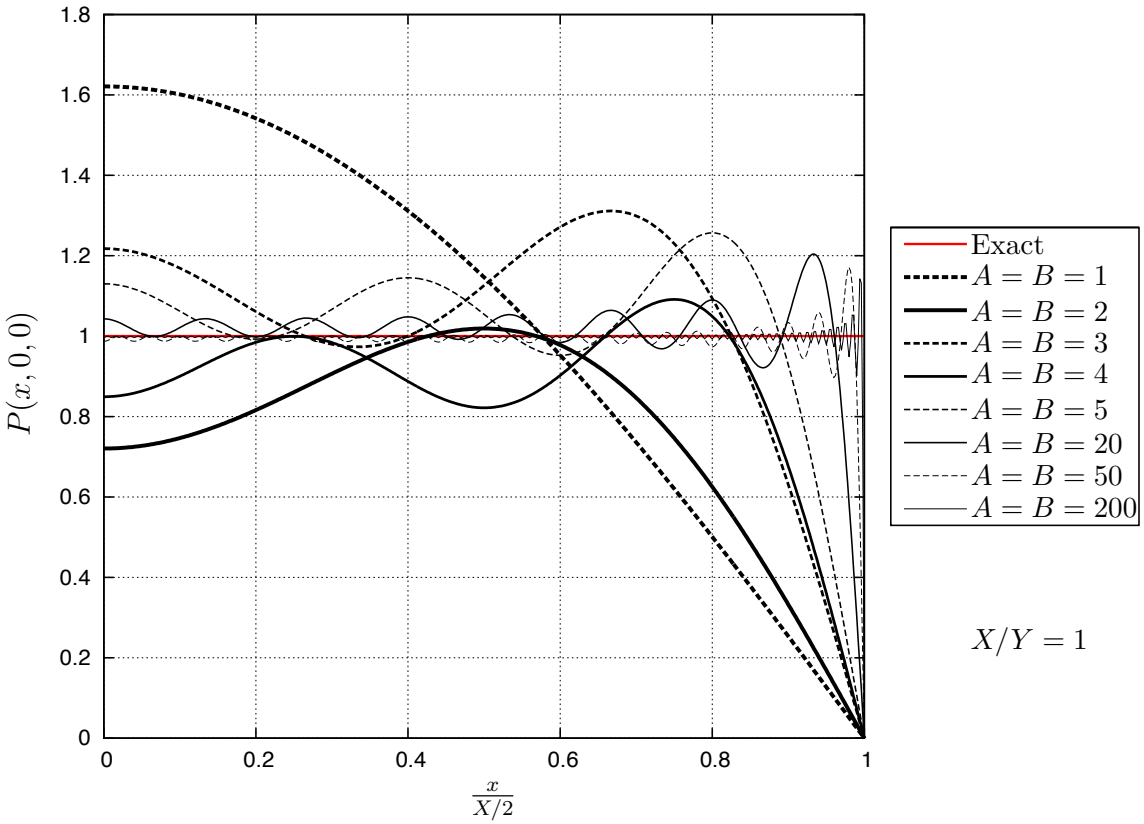

Figure 6.11: Eigenfunction Expansion "Initial" Condition in 2-D Slab for Varying Equal Mode Expansions in Each Dimension

While reducing the number of modes in one direction dampens the oscillations, it also reduces the uniformity in that direction and therefore leads to convergence on a uniform value in the other direction that is not the actual "initial" condition. Figure 6.12 demonstrates this behavior.

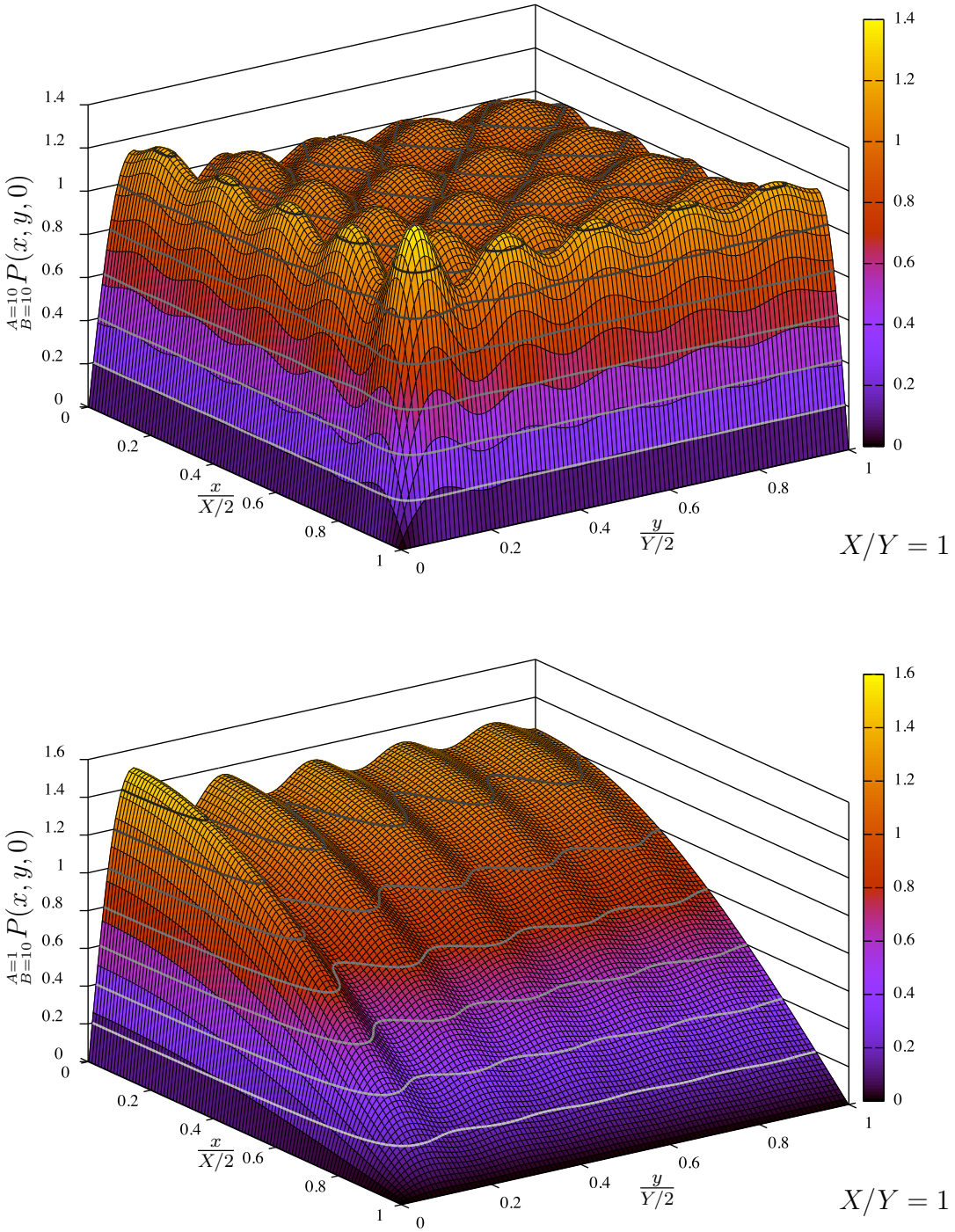

Figure 6.12: "Initial" condition in a 2-D Slab for Various Expansion Combinations

Based on the examination of various 1-D geometries, it is expected that the introduction of an additional finite dimension will increase the maximum relative modal error compared to a 1-D slab for a given τ, k_{eff}, and J. Figure 6.13 confirms this expectation.

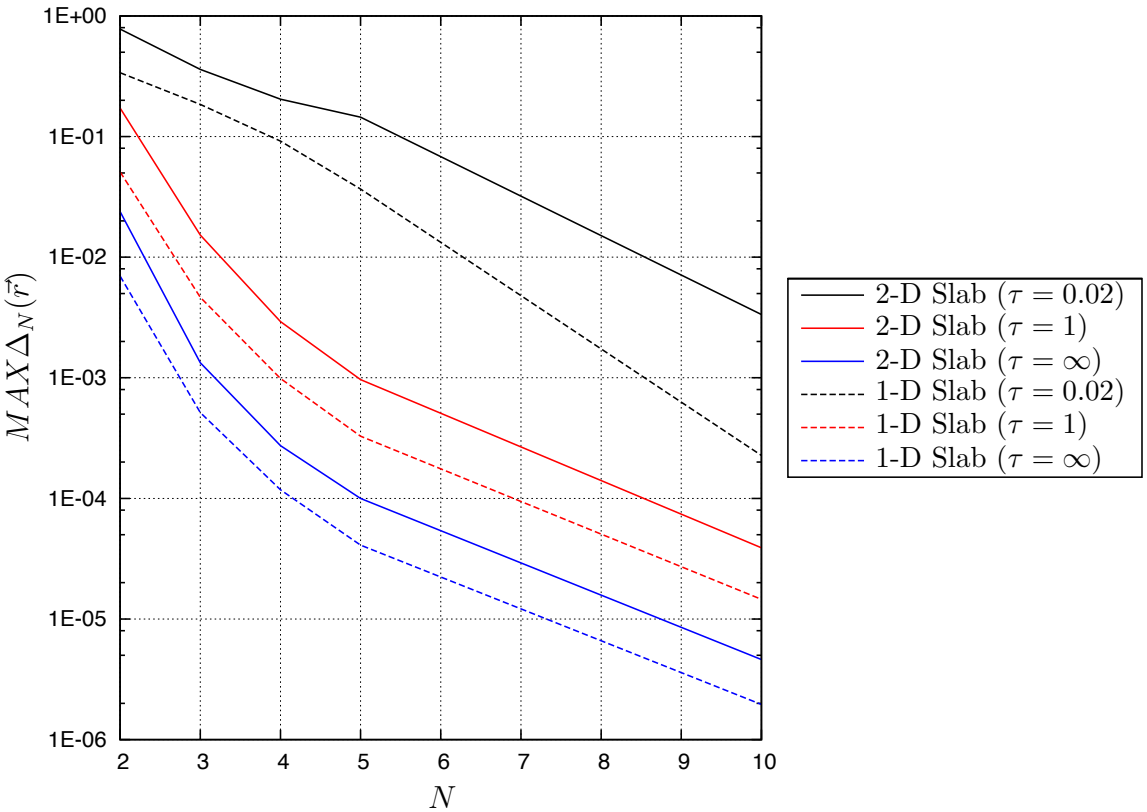

Figure 6.13: Maximum Relative Modal Error in P for Varying τ, N, and Geometry ($k_{eff} = 1.05$ & $J = 2$)

Examination of a 2-D slab with equal side lengths has produced the expected results. That an increase in finiteness increases the magnitude of the survival probability for a given τ, k_{eff}, and J has been shown to apply generally.

However, as has been noted, the relative modal error of a given expansion is not just a function of the magnitude of the survival probability, but of the relative uniformity in the shape of the survival probability as well. In 1-D cases, this uniformity

is a function of τ and k_{eff}. The extension into extra dimensions affords additional variability in the shape of the medium, and the uniformity of the survival probability is also a function of that shape.

While for the "initial" condition varying the ratio of the side lengths has no impact on the shape of the survival probability beyond scaling the dimensions, in the equilibrium and interim states the impact is more significant. This impact is most easily demonstrated by considering the POI in a 2-D slab where one side length is much greater than the other (i.e., $Y >> X$) in comparison to a slab where they are the same (i.e., $Y = X$).

For the oblong case, as Y grows, it becomes effectively infinite in extent as viewed from the solution in the x direction at $Y = 0$. The solution in the x direction ought to therefore approach the corresponding 1-D solution while the local solution in the y direction should be uniform in magnitude. As has been shown, however, many modes are needed to represent a uniform value well. As a consequence, the magnitude of the solution in the x direction oscillates with the solution in the y direction.

For the square case, the solution in each direction should more closely resemble that of the fundamental mode, as shown by the accuracy of the the fundamental mode approximation of the POI. Consequently, fewer modes are needed to represent the solution in each direction, and no such oscillation will be present.

These considerations demonstrate anew that the impact that increasing the number of modes in an expansion has on its accuracy is not simply a function of the magnitude of the survival probability, but of uniformity of the shape of the survival probability in a given dimension.

Figure 6.14 shows these behaviors by presenting a comparison between the POI in two slabs of equivalent k_{eff} but of varying X/Y ratios.

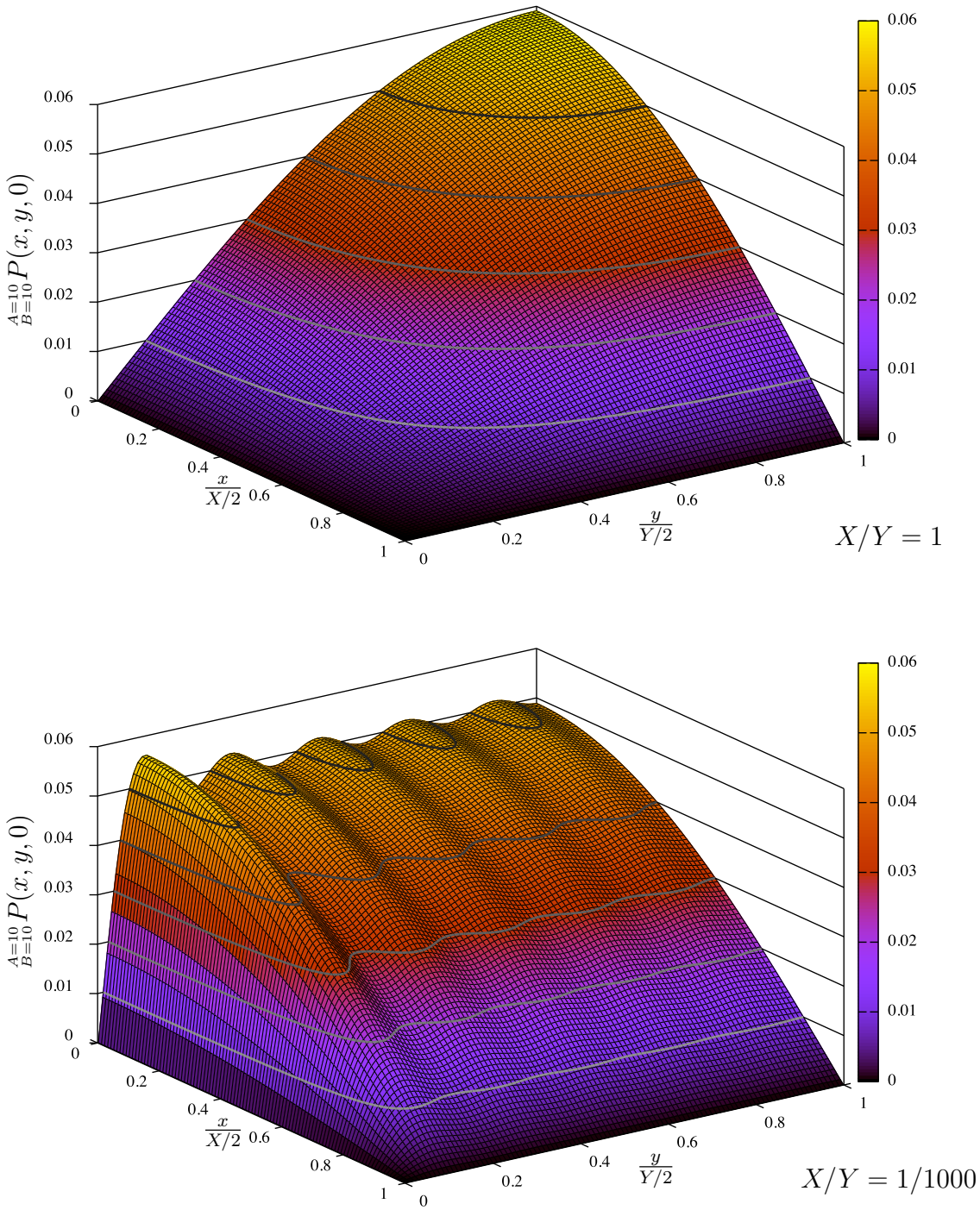

Figure 6.14: POI in a 2-D Slab for Various X/Y Ratios ($k_{eff} = 1.05$ & $J = 2$)

Although this behavior is undesirable, it is both expected and a predictable function of the shape of a given system.

Though convergence on the POI requires approximately the same number of neutron lifetimes as the 1-D cases for a given k_{eff}, shown in Figure 6.10, the computational burden is significantly greater for a given number of modes in each dimension. This comes as no surprise given the dramatic increase in the number of differential equations that must be solved.

Though the parameter space is increased, and the complexity is therefore correspondingly enhanced, it is clear that multi-dimensional EFE performs as expected.

6.6 Linear Stability Analysis of the Steady-State Eigenfunction Expansion Solutions

Use of the eigenfunction expansion technique has an additional benefit. It makes accessible a method for performing a linear stability analysis of the equilibrium solution. The fact that the POI is converged upon monotonically by solving the system of equations represented by Eq. (6.10) builds confidence that the steady-state solution is stable. That the POIs matches extremely well with the semi-analytical POIs and steady-state EFE POIs reinforce that confidence. Still, a more rigorous means of ascertaining the stability, or lack thereof, of the POI is desirable. To this end, a linear stability analysis of the eigenfunction expansion can be performed.

This is accomplished by introducing a small perturbation, t_n, to the steady-state solution, $\bar{T}_n$, and then allowing the system to evolve in time. The Hartmann-Grobman Theorem guarantees the stability of the original steady-state, $\bar{T}_n$, provided the perturbations diminish to zero [19].

As will be shown, if the perturbations grow, the solution is unstable. If they decay to zero, the solution is stable.

First, the perturbation is introduced :

$$T_n(\tau) = \bar{T}_n + t_n(\tau) \tag{6.20}$$

To determine whether or not the perturbation will grow or diminish, it must be differentiated with respect to time :

$$\frac{dt_n}{d\tau} = \frac{dT_n}{d\tau} - \cancelto{0}{\frac{d}{d\tau}\bar{T}_n}$$

$$= f_n(T_1, T_2, \cdots, T_n, \cdots, T_N) \tag{6.21}$$

Eq. (6.20) is then substituted into Eq. (6.21) :

$$f_n(T_1, T_2, \cdots, T_n, \cdots, T_N) = f_n\left(\bar{T}_1 + t_1, \bar{T}_2 + t_2, \cdots, \bar{T}_n + t_n, \cdots, \bar{T}_N + t_N\right) \tag{6.22}$$

Eq. (6.22) is then expanded in a Taylor series. Because the perturbations are small, the nonlinear terms are in turn vanishingly small. The Taylor series is therefore truncated after the linear terms :

$$f_n(\cdots, T_N) = f_n\left(\cdots, \bar{T}_N\right) + \frac{\partial f_n}{\partial T_1}\left(\cdots, \bar{T}_N\right) t_1 + \frac{\partial f_n}{\partial T_2}\left(\cdots, \bar{T}_N\right) t_2 + \cdots$$

$$\cdots + \frac{\partial f_n}{\partial T_n}\left(\cdots, \bar{T}_N\right) t_n + \cdots + \frac{\partial f_n}{\partial T_N}\left(\cdots, \bar{T}_N\right) t_N \tag{6.23}$$

The series of N equations represented by Eq. (6.23) may be represented more conveniently using the Jacobian matrix of the original system of equations :

$$\begin{bmatrix} f_1 \\ f_2 \\ \vdots \\ f_n \\ \vdots \\ f_N \end{bmatrix} = \begin{bmatrix} \frac{\partial f_1}{\partial T_1} & \frac{\partial f_1}{\partial T_2} & \cdots & \frac{\partial f_1}{\partial T_n} & \cdots & \frac{\partial f_1}{\partial T_N} \\ \frac{\partial f_2}{\partial T_1} & \frac{\partial f_2}{\partial T_2} & \cdots & \frac{\partial f_2}{\partial T_n} & \cdots & \frac{\partial f_2}{\partial T_N} \\ \vdots & \vdots & \ddots & \vdots & \iddots & \vdots \\ \frac{\partial f_n}{\partial T_1} & \frac{\partial f_n}{\partial T_2} & \cdots & \frac{\partial f_n}{\partial T_n} & \cdots & \frac{\partial f_n}{\partial T_N} \\ \vdots & \vdots & \iddots & \vdots & \ddots & \vdots \\ \frac{\partial f_N}{\partial T_1} & \frac{\partial f_N}{\partial T_2} & \cdots & \frac{\partial f_N}{\partial T_n} & \cdots & \frac{\partial f_N}{\partial T_N} \end{bmatrix} \begin{bmatrix} t_1 \\ t_2 \\ \vdots \\ t_n \\ \vdots \\ t_N \end{bmatrix} \tag{6.24}$$

If the eigenvalues of the Jacobian are all negative, the perturbations will all go to zero in time. If the largest eigenvalue is negative, it follows that all of the eigenvalues must be. Figure 6.15 presents these eigenvalues throughout the parameter space, assuring the stability of the steady-state solutions produced by EFE.

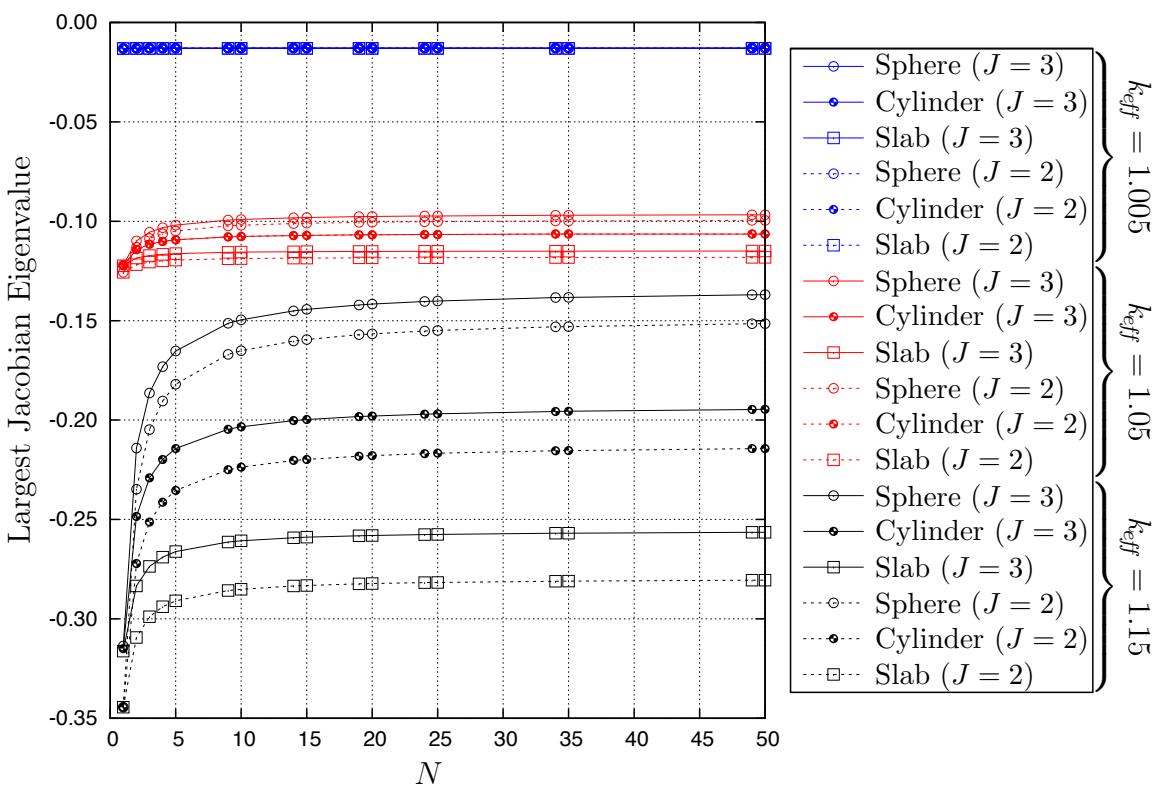

Figure 6.15: Largest Jacobian Eigenvalue for Varying Geometry, k_{eff}, J, and N

6.7 Conclusions from the Eigenfunction Expansion Solutions

Comparison of the eigenfunction expansion solutions in a one-dimensional slab to available analytical "initial" conditions and semi-analytical equilibrium solutions showed that the EFE technique is capable of representing the survival probability to the highest accuracies possible. Using the access to more complicated geometries afforded by EFE, the expected increase in the magnitude of the survival probability with increased finiteness for a given k_{eff} was confirmed.

Because the survival probability significantly decreases in magnitude and takes on a shape resembling a fundamental mode approximation very rapidly with the passage of survival time, EFE permits accurate integration over the entire survival time parameter space for problems where such integration might be needed.

The relative modal error, a measure of the accuracy afforded by additional modes in an expansion, was shown to be a function of the magnitude of the survival probability as well as the relative uniformity of the shape of the survival probability. Regardless of geometry, the number of factorial moments included in the equation serves to inform the magnitude of the survival probability, with additional even moments diminishing the magnitude and odd moments increasing it. As k_{eff} grows and τ approaches zero, the survival probability grows in magnitude and tends to become more uniform. In multi-dimensional problems, uniformity of the shape of the survival probability is also a function of the shape of the medium, with increasing profile uniformity in a given dimension for ratios of characteristic dimensions deviating from unity.

Being that both the computational burden and the solution accuracy associated with a given expansion is directly tied to the range of survival time being examined,

the system k_{eff}, the number of factorial moments included in the equation being solved, the number of modes in the expansion, and the shape of the medium hosting the particle chain, the EFE technique proves to be a powerful method of solution for time-dependent survival probability equations of arbitrary nonlinearity. Understanding the nature of the solution being sought based on expected behaviors allows users to deliberately tailor expansions, affording a highly capable, flexible, and easily manipulated balance of computational economy and solution accuracy. Additionally, EFE lends itself to a linear stability analysis of the equilibrium solution, confirming the stability of computed POIs.

Chapter 7

Conclusions and Future Work

7.1 Summary

Having begun with the one-speed, delayed neutron precursor-free, isotropic scattering form of the Pál-Bell Equation, a simplified equation for the neutron survival probability was developed by applying the well-known diffusion approximation. This approximation was implemented primarily to take advantage of the exact eigenfunctions that result from the linear portion of the equation in special geometries so that the efficacy of an eigenfunction expansion technique to solve the equation could be assessed.

Because the survival probability is defined by a nonlinear partial differential equation, characteristics of the survival probability were examined by approaching the problem with simplified forms of the survival probability equation. Though qualitative expectations of the impact that varying parameters has are accessible by Gedankenexperiment, accumulating the observations afforded by the simplified equations and using them to develop expectations for the system behavior enabled complexity to be reintroduced with confidence, and in a measured way.

While the quadratic approximation affords a number of analytical expressions describing the survival probability, more nonlinear terms must be preserved for larger values of the survival probability to achieve given accuracies. Because the "initial" condition of the survival probability demands large values, solution by numerical methods is necessary for high accuracy time-dependent solutions where small survival times are of interest. Additionally, for systems of large k_{eff}, the accuracy of the quadratic solutions will be compromised regardless of the survival time range being investigated.

To enable examination of equations of arbitrary nonlinearity for space and time-dependent problems, an eigenfunction expansion technique was developed and characterized. It was found to enable very high accuracy throughout an immense parameter space. Its demonstrated flexibility in terms of offering a broad spectrum of accuracy versus computational effort emphasizes the value of developing expectations of the solution behavior prior to computing the solution.

In the most general terms, the survival probability decreases in magnitude with increasing survival times, and increases with increasing k_{eff}. Solution accuracy is dependent on the magnitude of the survival probability in that the magnitude dictates the impact that preserving additional factorial moments of fission multiplicity will have as well as the relative modal error of eigenfunction expansion solutions. Additionally, the dimensions of the medium and range of survival time impact not only the magnitude of the survival probability, but the amount of uniformity in the shape of the survival probability. In the steady-state case, Bell's posit that the fundamental mode approximation does well to represent the probability of initiation for systems that are only modestly supercritical has been positively confirmed. To first order, it provides a decent approximation for even high values of k_{eff}.

By understanding these concepts, the eigenfunction expansion technique can be deliberately crafted to achieve a desired accuracy and minimize the effort expended.

7.2 Future Work

The intent of this work was largely to validate that eigenfunctions of the linear portion of the survival probability equation can be used to construct the time and space-dependent survival probability. To more easily demonstrate this, the diffusion approximation was utilized. The validity of this approximation is limited, and extension to a full transport equation solution is therefore desirable as is extension to multiple energy group problems.

Applications and studies incorporating this technique include modeling criticality excursions and burst characteristics of certain reactors. Time-dependent cross-sections and intrinsic, random sources can be incorporated to facilitate such studies. Application to multiple region problems, such as would exist in most realistic configurations of interest, is another area for further development.

As discussed, computational effort can be minimized by designing the solution technique at the onset of the problem. Still, computational efficiency could be enhanced by implementing a mechanism to "throttle" the number of modes in an expansion when they aren't necessary to achieve the desired accuracy. In the same way, the number of nonlinear terms in the equation could be adjusted in a time-dependent fashion to achieve similar gains in efficiency. These sorts of utilities would be especially valuable in dynamic simulations, where material configurations could be changing rapidly.

With the benefit realized by existing simplified models of stochastic neutron transport problems, the work presented here provides a means of more accurate examination of a large class of problems where the neutron population is behaving stochastically.

References

[1] I. Pázsit and L. Pál, *Neutron Fluctuations: A Treatise on the Physics of Branching Processes*. Oxford, UK: Elsevier Ltd., 2008.

[2] G. Hansen, "Assembly of Fissionable Material in the Presence of a Weak Neutron Source," *Nuclear Science and Engineering*, vol. 8, pp. 709–719, 1960.

[3] A. Prinja and F. Souto, "Probability distribution for neutron multiplying systems without delayed neutrons," LA-UR-09-07886, Los Alamos National Laboratory, 2009.

[4] G. Bell, "On the Stochastic Theory of Neutron Transport," *Nuclear Science and Engineering*, vol. 21, pp. 390–401, 1965.

[5] L. Pál, "Statistical theory of neutron chain reactions," in *Third International Conference on the Peaceful Uses of Atomic Energy*, vol. 2, (Geneva, CH), pp. 218–228, International Conference on the Peaceful Uses of Atomic Energy, 1964.

[6] G. Bell and C. Lee, "On the Probability of Initiating a Persistent Fission Chain," LA-2608 (Deleted), Los Alamos National Laboratory, 1976.

[7] R. Baker, "Deterministic methods for time-dependent stochastic neutron transport," in *International Conference on Mathematics, Computational Methods, and Reactor Physics*, (Saratoga Springs, NY), pp. CD–ROM, American Nuclear Society, 2009.

[8] S. Ramsey and G. Hutchens, "Approximate Solution and Application of the Survival Probability Diffusion Equation," *Nuclear Science and Engineering*, vol. 170, pp. 1–15, 2012.

[9] J.J. Duderstadt and L.J. Hamilton, *Nuclear Reactor Analysis*. Hoboken, NJ: John Wiley and Sons, Inc., 1976.

[10] G.I. Bell and S. Glasstone, *Nuclear Reactor Theory*. Malabar, FL: Robert E. Krieger Publishing Co., Inc., 1970.

[11] A.F. Henry, *Nuclear Reactor Analysis*. Cambridge, MA: MIT Press, 1975.

[12] Los Alamos National Laboratory, "NJOY 2010 Nuclear Data Processing System," Accessed : October 2011. http://t2.lanl.gov/codes/NJOY10/index.html.

[13] Los Alamos National Laboratory, "ENDF/B-VII Incident Neutron Data," Accessed : October 2011. http://t2.lanl.gov/data/neutron7.html.

[14] J. Lestone, "Energy and isotope dependence of neutron multiplicity distributions," LA-UR-05-0288, Los Alamos National Laboratory, 2005.

[15] L.F. Shampine and M.W. Reichelt, "The MATLAB ODE Suite," *SIAM Journal on Scientific Computing*, vol. 18, pp. 1–22, 1997.

[16] L.F. Shampine, "Vectorized Adaptive Quadrature in MATLAB," *Journal of Computational and Applied Mathematics*, vol. 211, pp. 131–140, 2008.

[17] G. Arken and H. Weber, *Mathematical Methods for Physicists*. San Diego, CA: Academic Press, Inc., 1995.

[18] J. Ortega and W. Rheinboldt, *Iterative Solution of Nonlinear Equations in Several Variables*. Philadelphia, PA: SIAM, 2000.

[19] M. Tabor, *Chaos and Integrability in Nonlinear Dynamics : An Introduction*. New York, NY: John Wiley and Sons, Inc., 1989.